EFFECT OF MICROSTRUCTURE ON THE COLD HEADABILITY OF A MEDIUM CARBON STEEL

by

Xiaoyu Ma

Department of Mining, Metals and Materials Engineering
McGill University
Montreal, Canada

A Thesis Submitted to the Faculty of Graduate Studies and Research
in Partial Fulfillment of the Requirements for the Degree of
Master of Engineering

ACKNOWLEDGEMENTS

I would like to express my sincere gratitude to my project supervisor Prof. John J. Jonas for his continual guidance, valuable advice and supervision throughout the entire project. His knowledge and assistance were of great value. I additionally thank Prof. James Nemes for his support and advice. The help of Dr. Alan Humphreys with this thesis was also greatly valuable.

I wish to thank IVACO Rolling Mills for their support of this work, particularly Dr. Michel Hone and Dr. Nick Nickoletopoulos. Thanks are also due to Dr. Baohong Cao for his organization of the tested materials.

I am grateful to Lorraine Mello for her administrative help and Edwin Fernandez for his laboratory expertise.

On a personal level, I thank my parents, brother and sisters for their understanding and unconditional love. Finally I thank my wife and daughter, whose love, patience and support are very much appreciated.

ABSTRACT

Cold headability is the ability of a cylindrical metallic specimen to be shaped at high strain rate into the head of a bolt, screw or other cold-formed part without cracking. This property is material dependent and can be influenced by many factors such as chemical composition, surface condition, and microstructure. This project focuses on the effect of microstructure upon the cold headability of a medium carbon steel (1036M).

Six different microstructures were produced by various heat treatment conditions. Drop Weight Tower (DWT) tests, developed at McGill in 2000 by Dr. N. Nickoletopoulos, were used on samples of these materials. Visual inspection, metallographic and SEM analysis were performed to identify cracks on the surface of tested samples, and trace their cause. The axial and circumferential strains of tested samples were measured and the strains at which cracks first occurred were used to assess the cold headability.

This research further indicates that DWT testing is a valid method for evaluating the cold headability of metallic materials and that the cold headability is particularly sensitive to the microstructure of a material.

RÉSUMÉ

La forgeabilité à froid est l'habilité d'un spécimen métallique cylindrique d'être formé à haut taux de déformation dans la tête d'un boulon, vis ou autre pièces produite par formage à froid sans fissuration. Cette propriété est dependante du matériau et peut être influencée par plusieurs facteurs comme la composition chimique, l'état de surface et la microstructure. L'emphase de ce projet est l'étude de l'effet de la microstructure sur le refoulage à froid d'un acier à teneur moyenne en carbone (1036M).

Six microstructures différentes ont été produites par divers traitements thermiques. L'essai de frappe développé à l'Université McGill en 2000 par le Dr. N. Nickoletopoulos, a été utilisé sur les divers échantillons. Des inspections visuelles, métallographiques et analyses au microscope à balayage ont été utilisés pour identifier les fissures à la surface des échantillons testés et d'identifier leurs causes. Les déformations axiales et circonférentielles des échantillons testés ont été mesurées et les deformations où les fissures débutent ont été utilisées pour décrire le refoulage à froid.

Cette recherche indique que l'essai de frappe est une méthode valide pour évaluer le refoulage à froid des matériaux métalliques, et que le refoulage à froid est particulièrement sensible à la microstructure du matériau.

TABLE OF CONTENTS

LIST OF FIGURES

LIST OF TABLES

Chapter 1

Introduction

Cold heading is a forging operation that is widely employed in the fastener industry to manufacture bolts, screws, and various fasteners. This operation involves an impact force applied to an end of a metal workpiece, to deform it into a designed contour. The most commonly used materials in the fastener industry are cold heading quality (CHQ) steels, including low carbon, medium carbon, and alloy steels.

However, some workpieces fail during the cold heading operation. These failures can be attributed to external reasons, such as die design and lubrication, or to properties of the material itself, known as cold headability.

The cold headability of steels can be affected by chemical composition, surface condition and microstructure. In general, steels are delivered to the fastener industry in the as-hot rolled state, of which the microstructure consists of ferrite and laminar pearlite. Laminar pearlite has a higher deformation resistance and less ductility, due to laminar cementite dividing a continuous matrix of ferrite. For medium carbon and alloy steels, a heat treatment is conducted before cold heading to optimise the microstructure for cold headability.

Conventional test methods to determine the workability of cold heading materials mainly involve traditional tensile and compression testing. However, although these methods are widely employed in the fastener industry, they are

not able to successfully assess the cold headability of materials. Their primary weakness is that the strain rate of the test does not represent that of the cold heading operation.

Previous workers [e.g. Nickoletopoulos 2001] have developed a Drop Weight Test (DWT) method for cold headability assessment. The DWT simulates the deformation occurring in the cold heading operation by dropping a weight to impact the sample being tested. The strain rate of the DWT can be as high as $800s^{-1}$ and is varied by changing the dropping height and specimen aspect ratio. The cold headability is assessed by measuring the strain at which a crack initiates.

In the present work, as a further development of this test method, a medium carbon CHQ steel, grade 1036M, was investigated. This research focused on the effect of microstructure on the cold headability. Two initial microstructures were used: as-hot rolled and heat treated, and four additional microstructures were produced through further heat treatment in the lab. DWTs were performed on samples of all six microstructures. The fracture strain at which a crack initiated was measured for the assessment of cold headability. Optical microscope (OM) and scanning electron microscope (SEM) observations were conducted to evaluate the effect of microstructure on the cold headability.

The specific objectives of the present project were:

- To verify the validity of the DWT on the different microstructures of a medium carbon steel; and

- To determine the effect of microstructure on the cold headability of a medium carbon steel.

This thesis is divided into the following chapters:

Chapter 2 presents a literature review, including a description of the definition of cold headability and its methods of assessment. Fracture mechanisms and the effect of microstructure on fracture are also reviewed in this chapter.

Chapter 3 explains the details of the experiments conducted.

Chapter 4 presents the experimental results including those pertaining to heat treatment and the DWT.

These results are discussed in Chapter 5.

Conclusions are presented in Chapter 6.

Chapter 2

Literature Review

2.1 The Cold Heading Process

Cold heading is a forging operation that is performed without an external heat source to preheat the material. In the course of cold heading, a force is applied to the free end of a metal workpiece, which is held between a die and a punch, to form the metal into a predetermined contour. It is widely employed in the fastener industry, where the end or a head of a metal blank is plastically deformed to produce fasteners such as bolts, screws, and so on [Nickoletopoulos, 2001; Wick, 1960]. A typical sequence of operations performed in the cold heading operation is indicated in Figure 2.1.

The production of fasteners involves quite sophisticated processing steps. Hot rolled CHQ steels are heat-treated, depending on their chemical composition and hardness, before the cold heading process. The main purpose of this treatment is to decrease the hardness and increase the workability of the steels [Bickford and Nassar, 1998].

These heat-treated CHQ steels are then descaled by either a mechanical or chemical method to remove oxide from their surface. Normally, pickling is performed on coiled material and hydrochloric, sulphuric, or hydrofluoric acid is used in the fastener industry. Then the materials are uncoiled, straightened, lime-coated, drawn and then cold headed. The cold heading operation can consist of

one or more strokes. This series of operations is performed continuously in a production line.

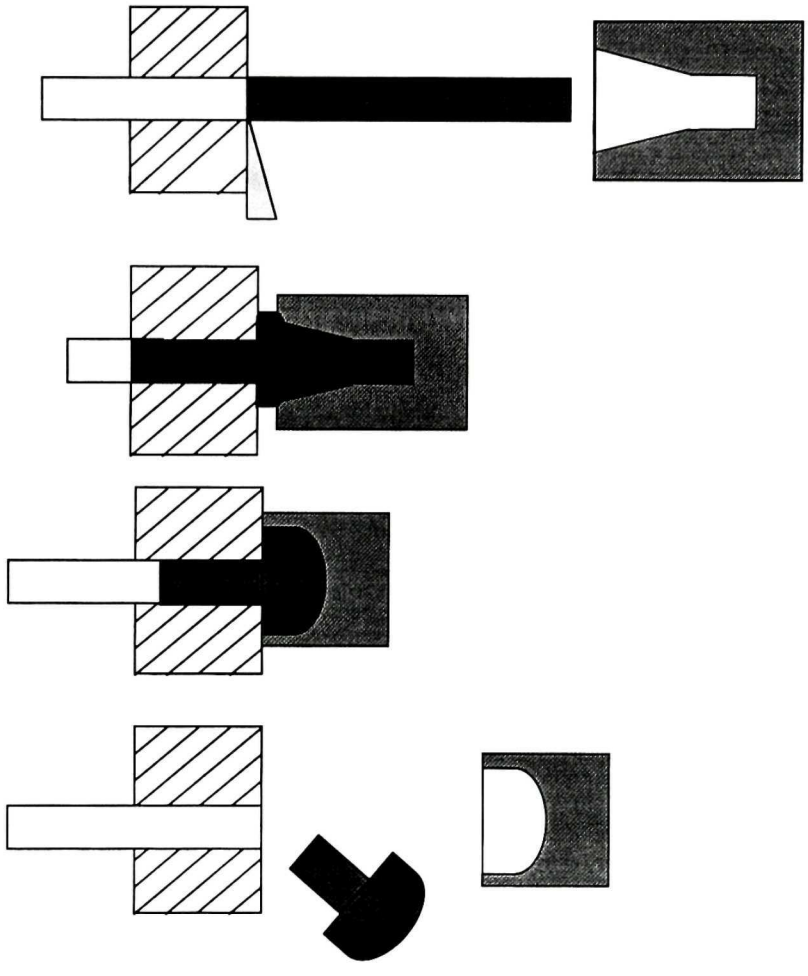

Figure 2.1 Typical sequence of operations performed in cold heading

After cold heading, the workpieces sometimes still need to be heat-treated, depending on the steel quality and technical and engineering requirements. A brief flowchart of a typical cold heading process is shown in Figure 2.2 [Sarruf, 2000].

2.2 CHQ Steel and Cold Headability

2.2.1 CHQ Steel

Although many kinds of metallic materials can be employed for the manufacture of fasteners, no other material offers the high strength at low cost that can be achieved by steel. For this reason, steel has always been the major material for manufacturing fasteners worldwide. Steels whose characteristics are specially developed for the purpose of cold heading are known as cold heading quality (CHQ) steels [Bickford and Nassar, 1998].

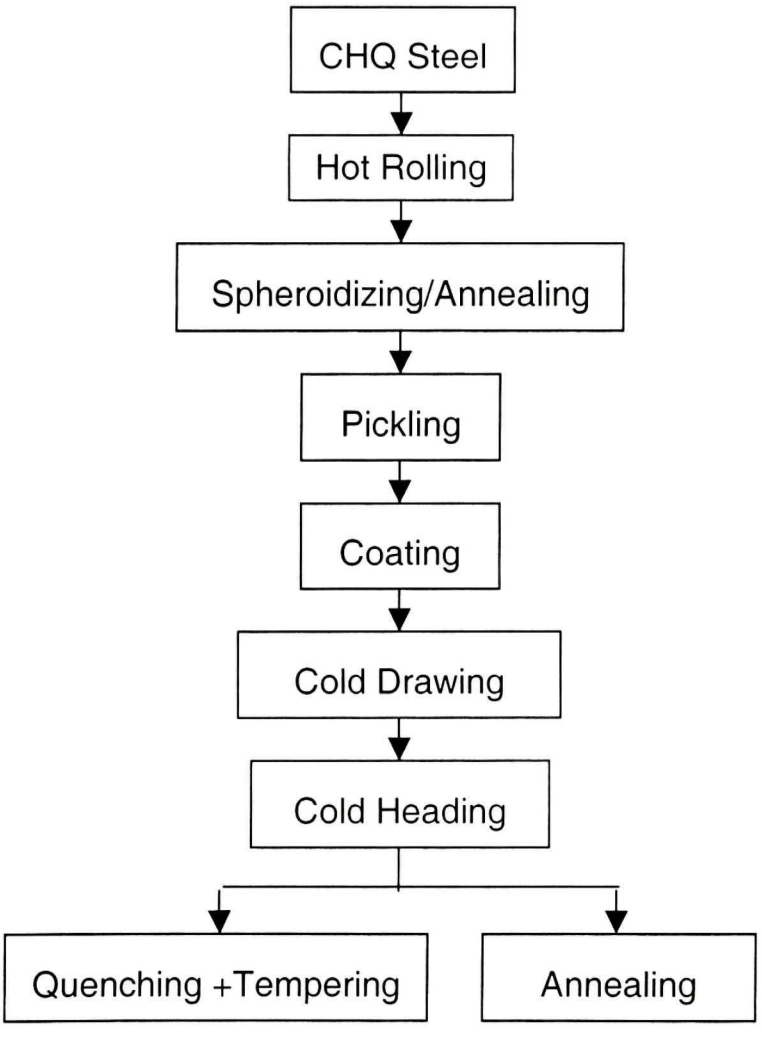

Figure 2.2 Brief flowchart of the cold heading process [Sarruf, 2000]

According to the strength grade of the fasteners produced, the steels used for cold heading can be either plain carbon or alloy types. Low carbon and medium carbon steels are often used for cold heading. Low carbon steel is generally used in the as-hot rolled state, whilst a heat treatment is normally applied to medium carbon steel before cold heading. In general, steels containing less than 0.08 or more than 0.45 wt.% carbon are seldom used for cold heading. When the diameter of fasteners becomes too large for carbon steels to provide homogeneous hardening through heat treatment, alloy steels are used. The selection of alloy steels depends on their hardening ability. However, high alloy steels are not chosen because of their greater strength and higher cost [Wick, 1960; Bickford and Nassar, 1998].

The ideal hardness for the raw material generally varies from 72 Rockwell B for low carbon steels to about 80 Rockwell B for medium carbon and alloy steels. In any case, the hardness cannot exceed 90 Rockwell B and material over this hardness may require annealing prior to cold heading. A spheroidized structure is generally preferred in medium carbon and alloy steels [Wick, 1960]

2.2.2 Cold Headability

Cold headability is the capability of a cylindrical piece of material to be shaped into the head of a bolt, screw, or other cold formed enlarged part, without cracking under the high strain rate imposed. It is a material-dependent property and is affected by the chemical composition and microstructure of the steels. Additionally, cold headability depends on the surface quality of the material and working conditions [Sarruf, 2000; Yoo, 1997].

Cold headability is expressed by the maximum strain achieved without generating a crack. The critical location for crack initiation in a cylindrical sample is at the barrel surface [Thibau, 1999]. Axial and circumferential strains are

usually used to measure cold headability. The measurement, as shown in Figure 2.3, can be conducted by measuring the space between grids on the surface of a sample, using the following relationship [Lee and Kuhn, 1973]:

Axial strain: $$\varepsilon_z = \ln\frac{h}{h_0} = \ln\frac{H}{H_0} \quad (1)$$

Circumferential strain: $$\varepsilon_\theta = \ln\frac{w}{w_0} = \ln\frac{D}{D_0} \quad (2)$$

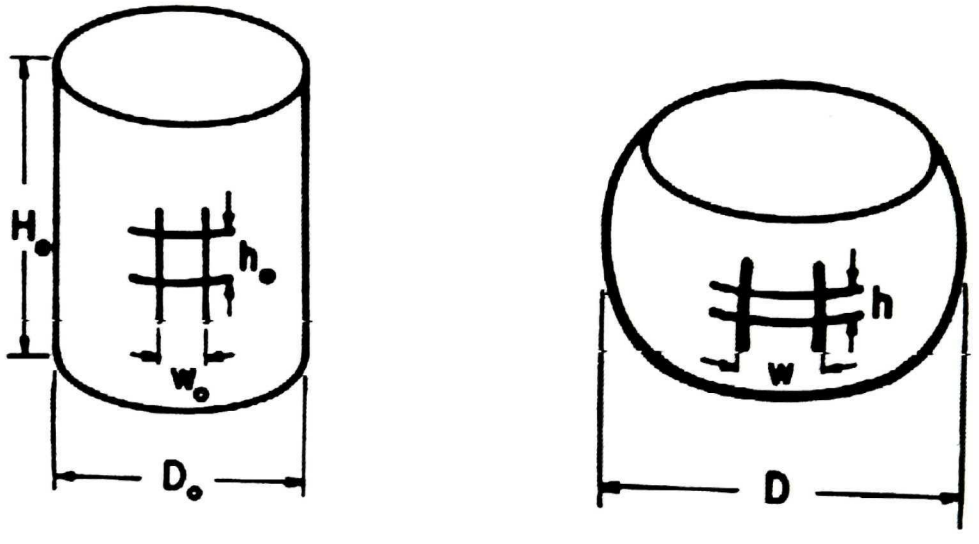

Figure 2.3 Strain measurement on compressed specimens [Lee and Kuhn, 1973]

The chemical composition is the strongest factor to influence cold headability. Cold headability is directly proportional to ductility. In general, raising the carbon content increases the yield and tensile strength, but decreases the ductility, impact and toughness properties of the steels. Therefore, high carbon content adversely affects the cold headability of a material [Nickoletopoulos, 2001].

Besides carbon content, alloy additions also affect the cold headability in a similar way to that of carbon. The investigation made by Muzak et al. [1995] showed a reduction of cold headability when the equivalent carbon content in the steels was increased. The equivalent carbon content (C_{eq}) is calculated by the equation:

$$C_{eq} = C + \frac{Mn}{6} + \frac{(Cr + Mo + V)}{5} + \frac{(Ni + Cu)}{15} \quad (3)$$

The presence of surface defects can influence a material's workability. It is believed that surface defects act as sources of circumferential stress concentration, which cause defects to open up during uniaxial compression. This results in ductile fracture at an earlier stage than would otherwise occur for specimens without defects. [Thomason 1969B; Jenner and Dodd, 1981]. Thomason reported that the defect depth is the primary factor to decrease the apparent ductility.

Microstructure is another factor that influences cold headability. Most CHQ steels are hypoeutectoid, with microstructures in the as-rolled state consisting of a ferrite matrix with varying amounts of lamellar pearlite. The most desirable microstructure for cold heading is a spheroidized microstructure, because this leads to higher ductility during processing [Matsunaga and Shiwaku, 1980].

Low carbon steels are soft enough to be cold-headed in the as-hot rolled state without prior heat treatment, whilst medium carbon and alloy steels have to be heat-treated before cold heading in order to decrease their hardness and hence improve their cold headability [Lehnert, 1995; Bickford and Nassar, 1998].

2.3 Typical Fastener Defects

The main defects that occur during cold heading operations are surface defects. Two types are commonly found on a fastener surface: longitudinal and oblique. Longitudinal defects are commonly found on the lateral surface of enlarged heading parts and are parallel to the longitudinal axis of fastener products. Oblique defects are shear cracks on the upset portion of a piece, typically at 45° to the longitudinal axis. Figures 2.4 and 2.5, respectively, show a longitudinal crack and an oblique crack present on the surfaces of the enlarged parts of two bolts.

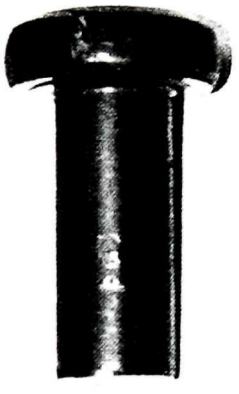

Figure 2.4 Longitudinal crack on the head of a bolt

Figure 2.5 Oblique crack on the head of a bolt

The cause of these surface defects is complicated. Nickoletopoulos [2001] believes that longitudinal cracks are due to the exhaustion of matrix ductility, whilst shear cracks are the result of localization induced by local softening and plastic instability.

Muzak et al. [1995] showed that a crack parallel to the longitudinal axis indicated the presence of a surface defect. A 45° shear crack signified that the plastic limit of the material had been reached.

Surface defects in cold heading materials can be initiated during previous processing, such as casting, and then elongated during subsequent rolling and drawing. If surface defects are present on a cold heading wire, ductile failure will occur at an early stage of the compression process. This is the result of the tensile surface stress, which has a strong influence on the ductility of cold heading wire, because the tensile stress acts normal to the longitudinal surface defects and mechanical fibreing. The effective stress concentration at the root of these defects will cause a large hydrostatic stress and severe localized straining, which can open up the defects and possibly produce cracks. If the cylindrical surface of cold heading wire is completely free from defects, ductile failure would eventually occur by shear fracture [Thomason, 1968].

Longitudinal cracking caused by surface defects occurs at a very early stage of compression, at low strain and prior to the presence of a shear crack. If a cylindrical specimen were compressed in the axial direction with very good lubrication to eliminate barreling, longitudinal defects would not be a source of rupture or fracture [Thomason, 1968].

2.4 Tests of Cold Headability

As explained above, cold headability is a function of many variables; thus, it is hard to assess cold headability by means of only one test. Conventional assessment involves tensile and simple compression testing to gauge yield and tensile strength, hardness, reduction of area and so on. These tests are easy to perform and represent the basic properties of the materials. However, there are some drawbacks in these conventional assessments. Firstly, these methods test

the samples at significantly lower strain rates than those involved in actual cold heading [Sarruf, 2000]. In fact, deformation at high strain rate is one of the most important features of the cold heading process.

Secondly, some researchers have pointed out that the tensile test is not suitable for the prediction of cold headability, because fracture in the tensile test does not initiate at the surface of the sample, as that in the cold heading operation. This is due to the change in the stress state once necking begins [Olsson, 1986].

Furthermore, the friction conditions associated with a conventional upset test are not similar to those that apply to cold heading. Also, the verification of failures appearing on the surface of the sample are visual and therefore subjective to the analyser [Muzak et al., 1995].

In order to overcome these problems, several new assessment methods have been developed. These have a common factor of simulating the deformation at a high strain rate.

2.4.1 Drop Weight Impact Test

One of the newly developed assessment methods is the drop weight impact test. The philosophy of this test is to deform the material to failure by an impact force and analyze the data acquired from the impact test. Figure 2.6 shows the principle of the test device. During a test, a wire specimen is held in an instrumented impact machine. The specimen diameter used on this device is 3.5 mm. The high speed instrumented impact tester is able to initiate up to 500 joules impact energy at a velocity of up to 7m/s. An impact force-displacement curve is recorded and the failure point can be identified, therefore the cold headability can be calculated. [Muzak et al., 1995].

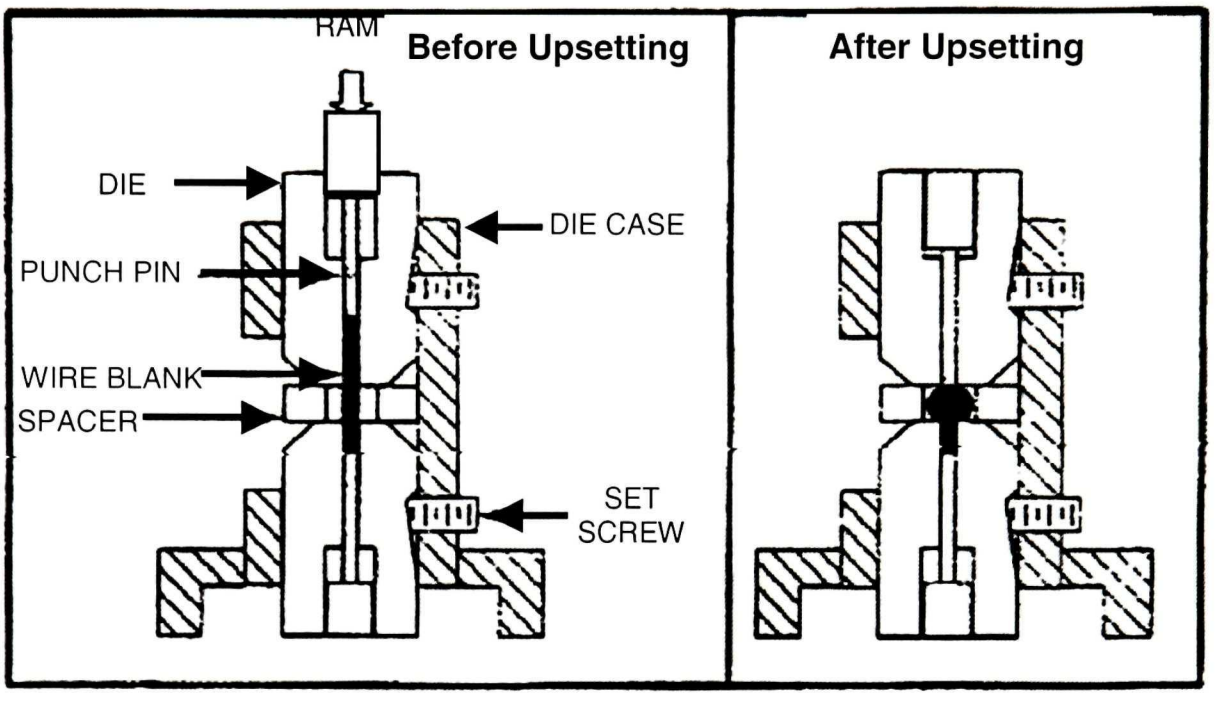

Figure 2.6 Drop weight impact test device [Muzak et al., 1995]

2.4.2 Split Hopkinson Pressure Bar Test

Another development to improve conventional assessment is the Split Hopkinson Pressure Bar Test, as shown in Figure 2.7.

This test consists of two pressure bars that are specially processed. One is known as the incident bar, the other is the transmitted bar. Strain gauges are attached to these and a lubricated specimen is mounted between them. The impact is provided by a striker bar, which is propelled by an air pressure gun. Upon impact, the elastic deformation of both the incident bar and the transmitted bar are recorded by the strain gauges. The deformation features of the sample, including the dynamic stress-strain curve, can be obtained via a computer program. By this method, an order of magnitude higher strain rates (as high as $10^3\ s^{-1}$) can be reached [Yoo et al., 1997].

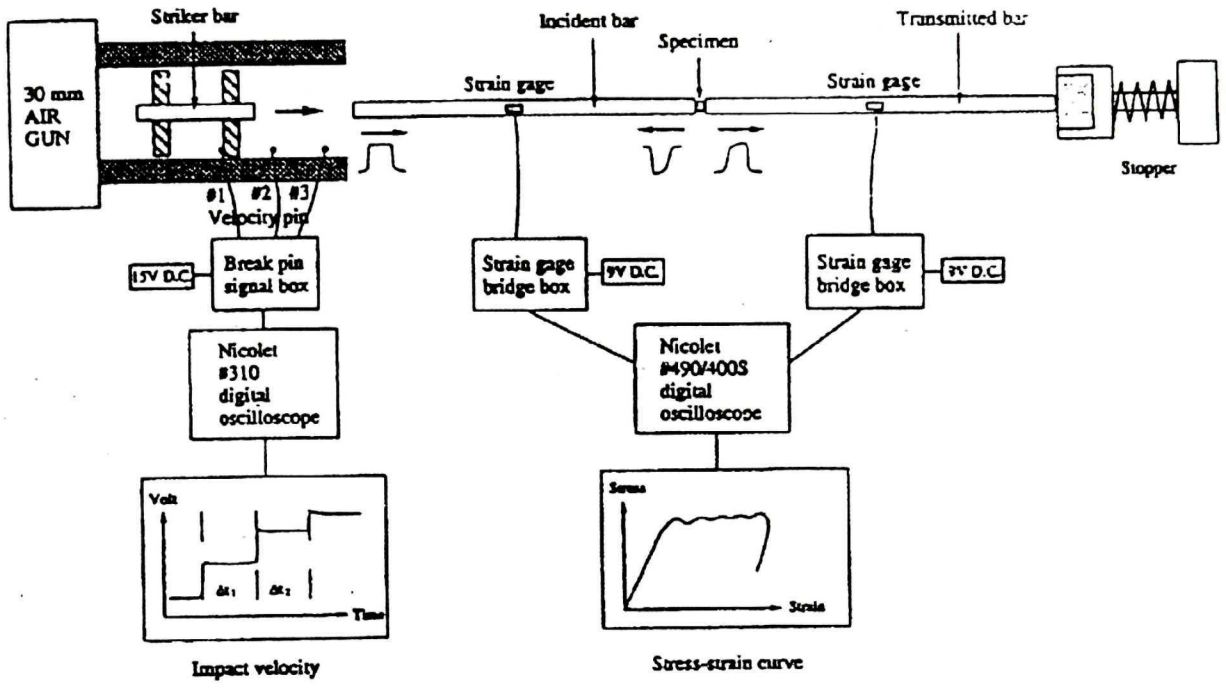

Figure 2.7 Schematic diagram of the Split Hopkinson Pressure Bar Test [Yoo et al., 1997].

2.4.3 Drop Weight Test

The drop weight test (DWT) machine, developed by Nickoletopoulos, simulates the deformation that occurs in the case of cold heading, by dropping a weight to impact the sample that is being tested. In general, it is similar to the design employed for the drop weight impact tester discussed in 2.4.1, but the present DWT machine can test a larger specimen diameter of 5.2mm.

The DWT machine consists of a tower enabling a set of weight plates to drop downward from a height of up to 2.5 meters onto a die set and stop blocks. Figure 2.8 shows the structure of the DWT machine and Figure 2.9 the details of the die set. The dropped weight impacts the die set, which transfers the impact

load from the crosshead to the sample. The whole die set configuration is mounted on a central column that is fixed to the base of the DWT machine [Nickoletopoulos, 2001].

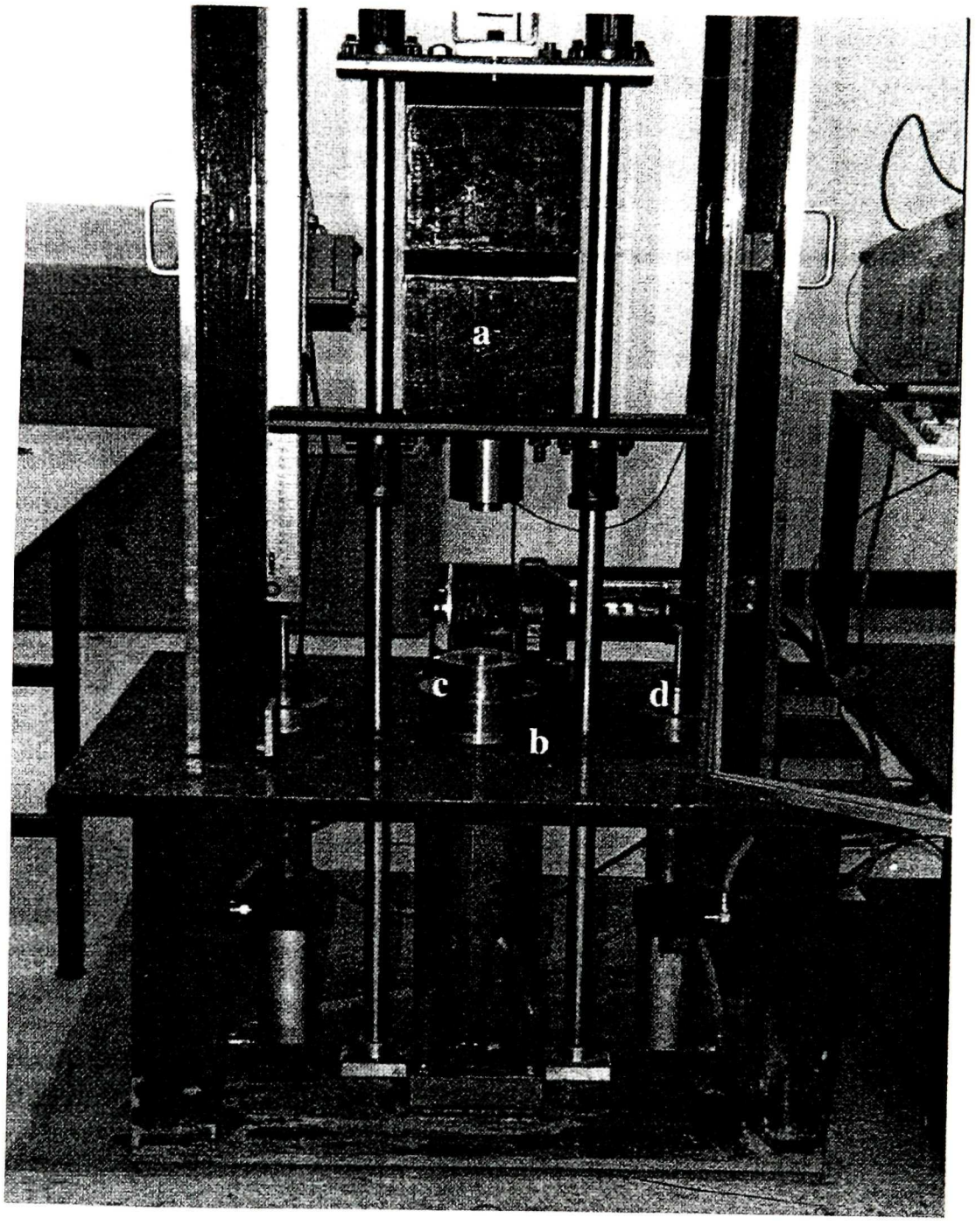

Figure 2.8 Structure of DWT machine (a) weight plates, (b) load cell, (c) die set configuration, (d) pneumatic shock absorbers

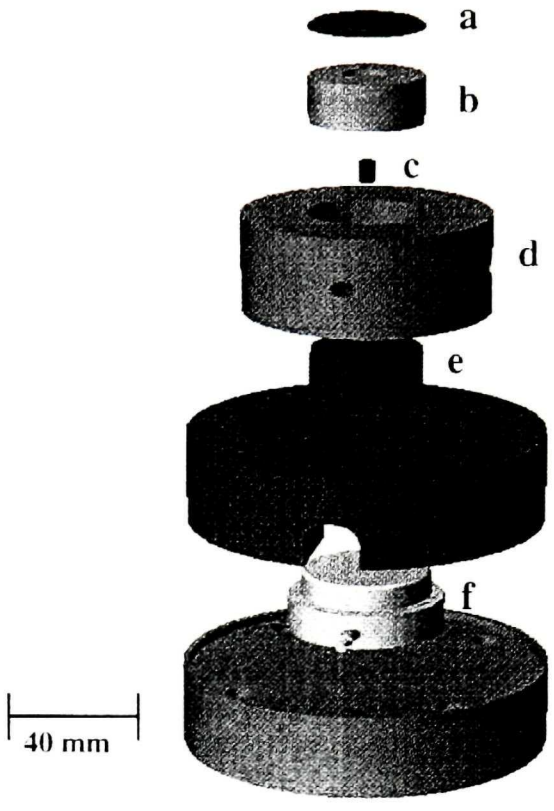

Figure 2.9 Exploded view of the die-set assembly for the DWT including: (a) die protection cap, (b) upper die, (c) test specimen, (d) die sleeve, (e) lower die, and (f) load cell.

A load cell, located between the die set and the central column, measures real time load and displacement data at the moment of impact. From these, a load vs. displacement curve can be obtained. The area below the curve is the energy that the sample absorbs during the impact period.

The impact load and strain rate are adjustable by varying the dropping weight and height. A sample can be deformed until failure occurs by cracking. The axial and circumferential failure strains of the sample are then measured. The minimum strain at which a crack starts is taken as the fracture strain, which is an indication of cold headability.

Nickoletopoulos [2001] has used the DWT to examine 7 heats of 1038 steel, with different nitrogen, copper and residual element contents, in both the as-hot rolled and spheroidized states. The diameter of the sample was 5.2 mm and an aspect ratio of 1.3 was chosen for all 7 heats, although one of the heats was additionally tested using ratios of 1.0 and 1.6. The samples of all 7 heats were cracked using a constant dropping height of 1.5 m at various weights from 11.8-26.3kg.

The tests demonstrated that the DWT simulated the cold heading process by generating an ideal (constant high strain rate) impact load. The load applied to the sample reached a maximum value within a very short time. Figures 2.10 and 2.11 show the load-time curves of the DWT for the as-hot rolled and spheroidized states, respectively. The load increased from zero to a maximum in around 0.002s, resulting in an approximate strain rate of $630s^{-1}$.

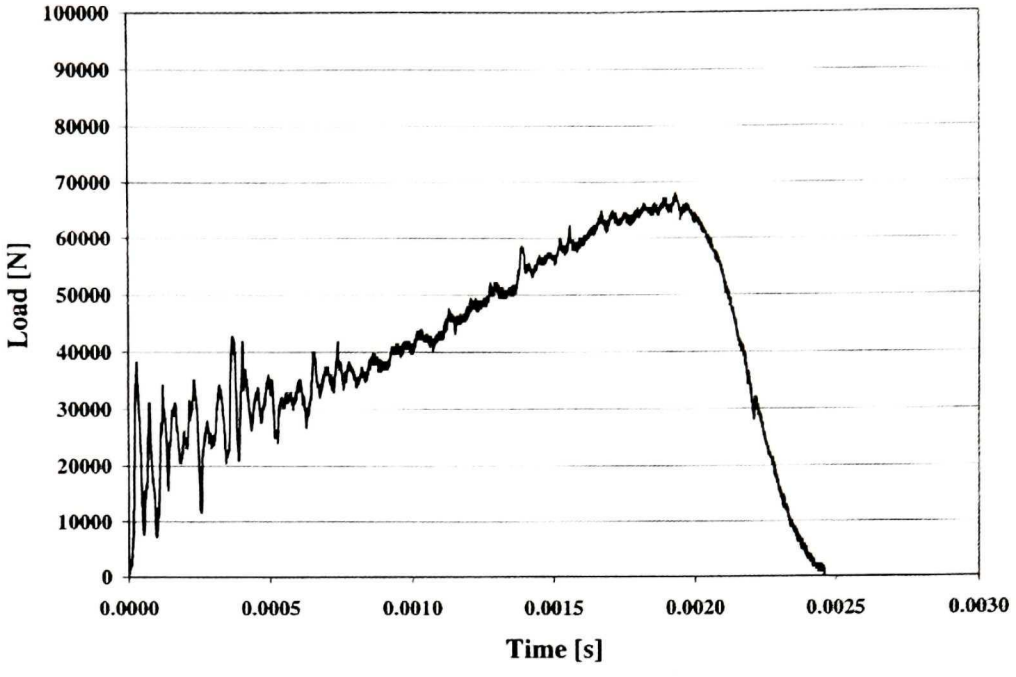

Figure 2.10 Load-Time curve of 1038 steel in the as-rolled state [Nickoletopoulos, 2001]

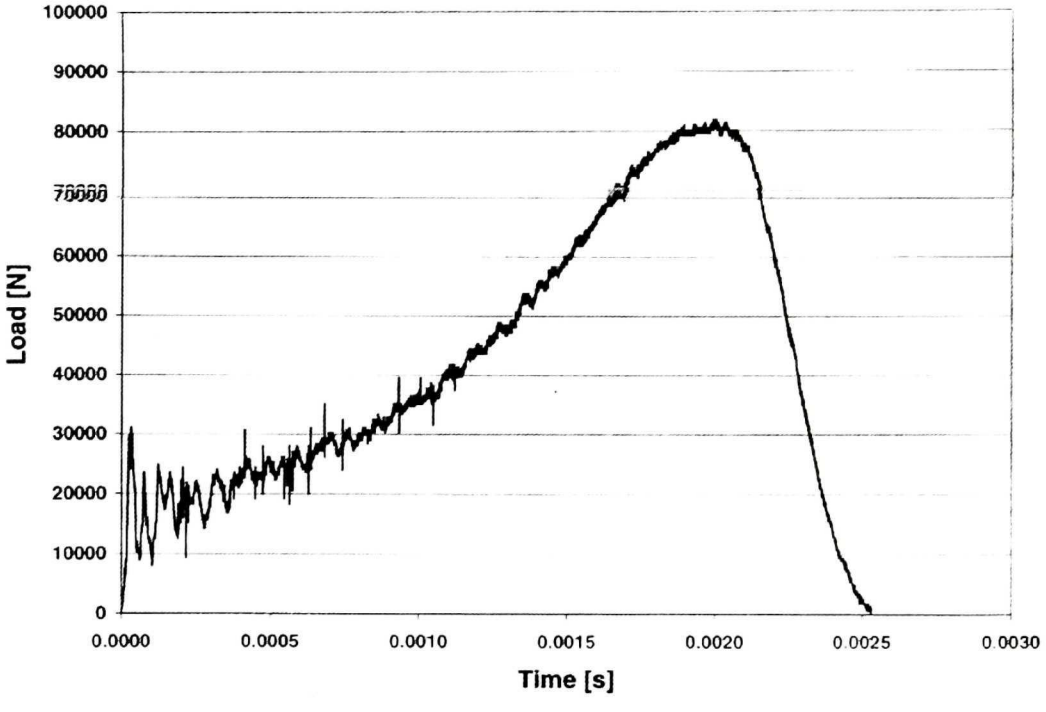

Figure 2.11 Load-Time curve of 1038 steel in the as-spheroidized state [Nickoletopoulos, 2001]

The approach to the maximum load has a steeper gradient for the spheroidized material than for the as-hot rolled state. This is due to the higher work hardening coefficient for the spheroidized material. This demonstrates that the DWT is able to identify feature differences associated with different microstructures.

Figure 2.12 shows a typical load-displacement curve of a DWT. Load-displacement curves are useful for analysis of the power impacted during loading.

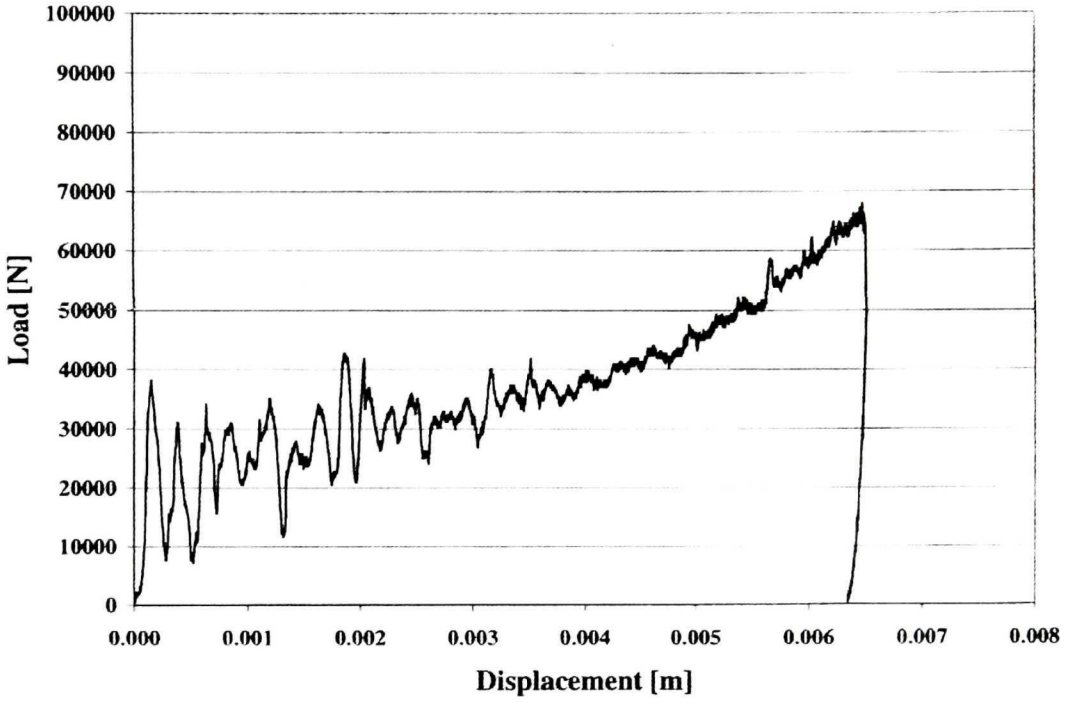

Figure 2.12 Load-displacement curve of as-hot rolled 1038 steel [Nickoletopoulos, 2001]

The transformation band, which is caused by rapid deformation heating and cooling, is a potential initiation site of internal cracks. Generation of this band requires a high strain rate and large deformation; therefore it is not easy to simulate this in the laboratory. However, Nickoletopoulos has successfully produced transformation bands in the DWT.

He concluded that the DWT is sensitive to the effect of surface integrity and microstructural differences between as-hot rolled and spheroidized materials on the fracture behavior during cold heading.

Therefore, the DWT is employed in the present work to evaluate the cold headability of the materials investigated. However, the load cell system was not used and the mechanical characteristics of the DWT were not researched in the present work.

2.5 Ductility Criteria

Ductility is defined as the ability of a material to withstand deformation without fracture. The apparent ductility of a workpiece depends on the stress and strain at the surface; once a crack appears at any position on the surface, the workability limit has been reached [Jenner and Dodd, 1981]. Cockroft and Latham [1968] proposed that when the work done by the maximum tensile stress reaches the critical value "C", ductile fracture will occur. This critical value is constant for a given material under the same conditions of heat treatment, test temperature and strain rate [Thomason, 1969]. The ductile criteria can be written:

$$\int_0^{\varepsilon_f} \sigma_1 d\varepsilon_{eq} = C \qquad (4)$$

σ_1 - maximum tensile stress

ε_f - fracture strain

$d\varepsilon_{eq}$ - effective plastic strain increment

C - critical value

During tensile testing, the maximum tensile stress acts along the centerline, whilst during upset deformation, the maximum tensile stress is located at the barrel surface in the circumferential direction [Nickoletopoulos, 2001].

The concept of forming limit diagrams, as shown in Figure 2.13, was developed to determine the criteria for fracture. A fracture line or fracture locus, that is a line joining each fracture point along different strain paths, is employed to predict fracture. The fracture line is parallel to the homogeneous compression line and has a gradient of –1/2. A material does not fracture at strains below the fracture line limit and fractures at strains above this line. This concept has been applied to various deformation processes such as upsetting, rolling and bending. Figure 2.14 shows the strain states in various deformation processes and Figure 2.15 the distribution of fracture points on the fracture line at different deformations. [Lee and Kuhn, 1973; Kuhn, 1977; Shah and Kuhn, 1986].

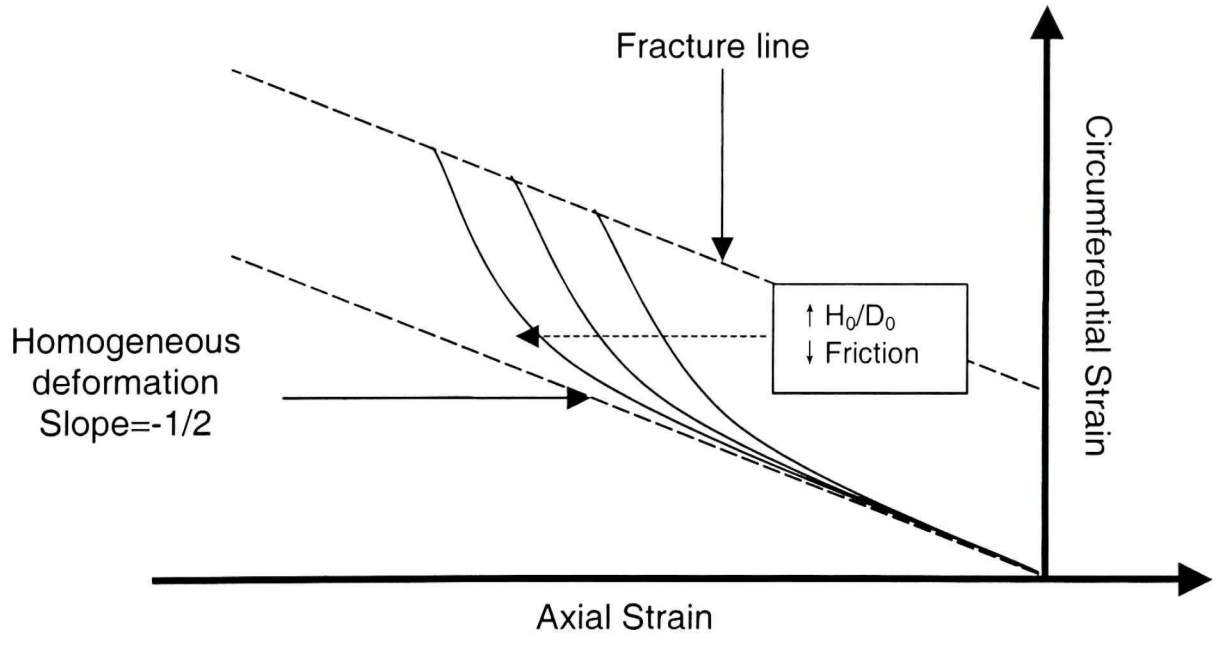

Figure 2.13 Forming limit diagram for upsetting test

The slope of the strain path has the greatest influence on the stress state at the free surface during upset deformation. When the slope equals –0.5 (homogenous deformation), the circumferential stress is zero. Under this situation, longitudinal defects will not be a source of fracture. For inhomogeneous deformation, the strain path gradient is greater than 0.5; thus the circumferential stress on the free surface is positive. The circumferential tensile stress greatly affects the workability, because the stress is normal to the longitudinal defects and mechanical fibers. This may therefore open up the defects and produce longitudinal cracking. [El-Domiaty, 1999].

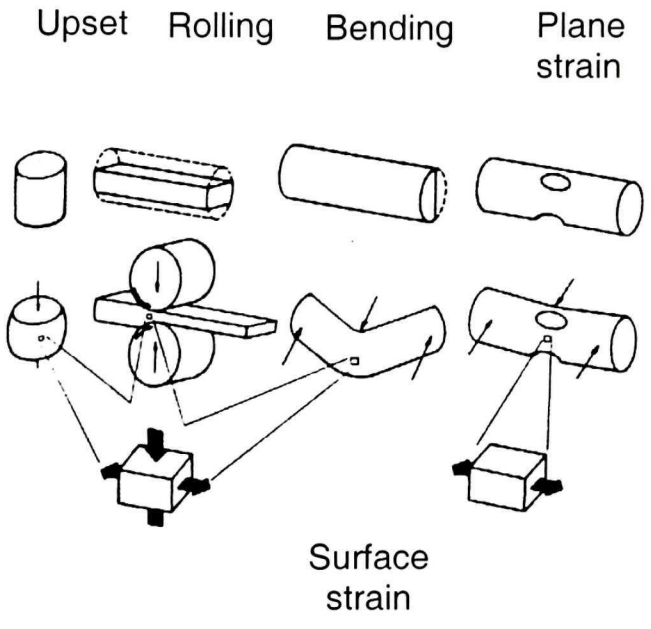

Figure 2.14 Surface strain states in various deformation processes

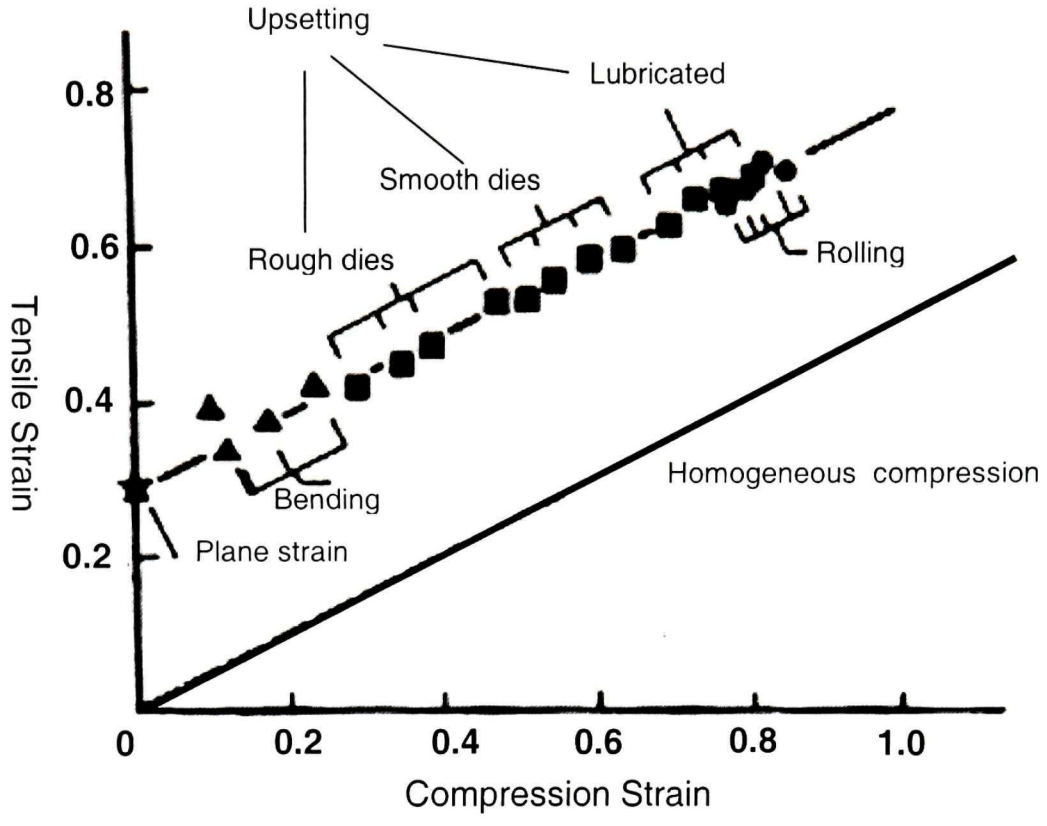

Figure 2.15 Distribution of fracture points on the fracture line at different deformations of 1045 steel [Lee and Kuhn, 1973]

El-Domiaty [1999] reported that the fracture line of AISI 1045 steel consisted of three line segments. The first segment was almost parallel to that of homogenous deformation (slope = –0.5), the second segment had a smaller gradient than the first, and the slope of the third segment was almost zero, as shown in Figure 2.16.

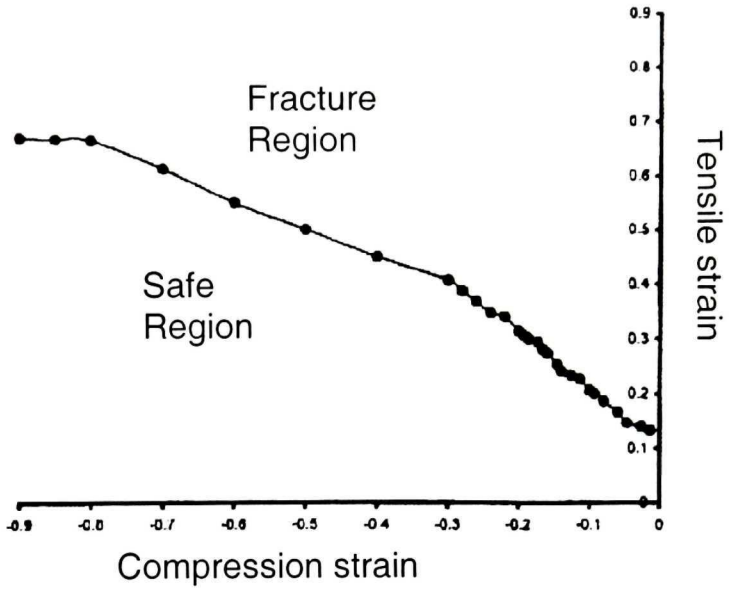

Figure 2.16 Fracture locus consisting of three segments for AISI 1045 steel [El-Domiaty, 1999]

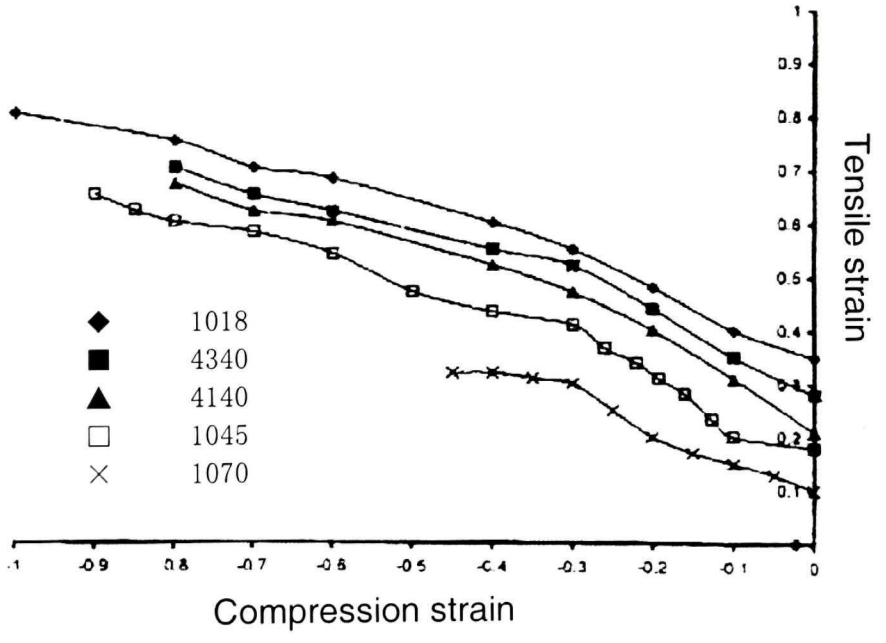

Figure 2.17 Fracture lines for steel containing different carbon and alloy contents [El-Domiaty, 1999]

The effect of carbon content on these fracture lines has been reported [El-Domiaty, 1999] for several steels containing 0.18-0.78 wt.% carbon. The results, as shown in Figure 2.17, indicate that the locus for the low carbon steel (0.18 wt.% C) is at the highest level in the forming limit diagram, whilst the high carbon steel (0.78 wt.% C) is located at the lowest level. This indicates that the low carbon steel has higher workability, together with a higher fracture strain, than the high carbon steel.

For some materials, fractures cannot be achieved in the lab, because the required fracture strains exceed the capacity of the test equipment. Thibau et al. [1999] developed a solution to this by introducing a notch into the surface of the sample. The fracture strain at a crack occurring at the root of this notch was then measured.

Thomason also introduced longitudinal grooves of various depths to the free surface of uniaxial compression specimens. During heading testing, cracks were initiated at the roots of these grooves. The critical depth of groove, which is defined as the minimum depth of the groove at which cracking occurs, was employed to measure the fracture criterion [Thomason, 1969/1970].

2.6 Ductile Fracture

Ductile fracture occurs in three stages: microvoid nucleation, growth of the microvoids with continued deformation and, finally, coalescence of the voids to produce complete fracture. [Magnusen et al., 1988; Maheshwari et al., 1978]. The total fracture strain, ε_f, is the sum of the strains of nucleation, growth and coalescence [Poruks et al., 1998]:

$$\varepsilon_f = \varepsilon_n + \varepsilon_g + \varepsilon_c \qquad (5)$$

where ε_n is the strain at which microvoid nucleation occurs, ε_g is the strain during which void growth developed, and ε_c is the strain during final coalescence [Poruks et al., 1998].

2.6.1 Microvoid Nucleation

Microvoid nucleation may occur on second phase particles by particle-matrix interface separation or by particle cracking. The second phase is usually less ductile than the matrix, so that the highest stress concentration is in this region. The voids nucleate preferentially at large particles, particularly at the tip of elongated precipitates [Gurland, 1972]. Fisher and Gurland, [1981] revealed that in low and medium carbon steels, voids occurred preferentially at particles located on grain boundaries. Interfacial decohesion generally occurred at particles of larger than average size. This is due to the fact that the critical stress for void nucleation at large particles is lower than that at small particles [Van Stone et al., 1985].

In low alloy steels, manganese sulphide inclusions are void nucleation sites at which interfacial decohesion is most frequently observed [Cox and Low, 1974]. Carbides are other commonly occurring void nucleation sites. The large carbides fail by cracking, whilst smaller carbides fail by interfacial decohesion [Cox and Low, 1974; Gurland, 1972].

The distribution of second phase particles affects void nucleation. Microvoid nucleation occurs more easily in microstructures with clusters of particles than those with homogeneous particle distributions. This is because the interparticle spacings in particle clusters are smaller than those in homogeneous structures. [Poruks, 1998]. Voids are often formed between closely spaced particles [Fisher and Gurland, 1981].

Void nucleation is a function of true plastic strain. Cox and Low [1974] have researched this relation in AISI 4340 steel and revealed that when the plastic strain reached a certain degree, voids were found at all inclusion particles. It is evident that void nucleation also depends upon the volume fraction of second phase particles. More second phase particles result in the formation of more microvoids.

Fisher and Gurland [1981] revealed that void nucleation in low and medium carbon spheroidized steels occurred preferentially by interfacial decohesion, whilst in high carbon spheroidized steel, the primary mode of void formation was particle fracture. The cracks were perpendicular to the applied stress direction in tensile samples and parallel to the loading direction in compression. At a given strain, void density increased with carbon content and decreasing cementite particle size [Gurland, 1972].

2.6.2 Growth of Voids

Void growth is the process of cavity enlargement by highly localized plastic deformation [Van Stone et al., 1985]. It has been estimated that more than 87% of the energy expended during the ductile failure of a high strength steel is absorbed during void growth [Shockey et al., 1977].

Cavity growth is controlled by the plastic flow of matrix material around the nucleation site and by the decohesion of smaller second phase particles. These voids tend to preserve a globular or ellipsoidal shape during growth if it is controlled by plastic flow of the matrix material, in order to minimize surface and local plastic energy [Floreen and Hayden, 1970]. Alternatively they can grow by repeated void nucleation and tearing along a path of neighboring particles. Voids exhibit irregular shapes if their growth is controlled by the decohesion of smaller second phase particles [Cox and Low, 1974]. It was revealed that voids grew

more rapidly in the high strength condition of a material than in the equivalent low strength condition [Floreen and Hayden, 1970].

2.6.3 Void Coalescence

Void coalescence is the last stage of ductile fracture. With continuing deformation, nucleated voids grow until they impinge on each other. Void impingement is one of the most common mechanisms of coalescence.

Secondary void formation may also occur in the bands of intense localized shear between large particle-nucleated voids. Sheets of these voids are produced in the bands connecting larger voids. These void sheets generally exhibit angles of 30-40° to the tensile direction [Van Stone et al., 1985].

Cox and Low [1974] revealed that in AISI 4340 steel, large voids may be formed by decohesion of the interface between the matrix and MnS inclusion particles. The growth of these voids was interrupted before impingement by the formation of void sheets at 45° to the tensile direction.

2.7 Improvement of Microstructure for Cold Heading

The as-hot rolled state of CHQ steels consists of ferrite and pearlite. Lamellar cementite subdivides the ferrite, causing deformation resistance and stress concentration in the structure. Spheroidized microstructures, which represent the most thermodynamically stable structures in steels, are comprised of spherical carbide particles uniformly dispersed throughout the ferrite matrix. This continuous matrix provides the softest and most ductile condition; thus it is the most desirable structure for cold heading operations [Muzak et al., 1995].

The purpose of a spheroidizing treatment is to obtain a microstructure of globular cementite distributed in a ferrite matrix. In general, spheroidizing annealing is performed closely above or just below the Ac1 temperature for a certain time after which the steel is cooled slowly to 600°C [Matsunaga et al., 1980]. According to whether the temperature is above or below the Ac1, two types of spheroidization may occur: these are known as the intercritical and subcritical processes.

2.7.1 Intercritical Process

The intercritical process is where the steel is initially heated to above the Ac1 temperature, then cooled down to below the Ac1 and held for a longer time [Muzak et al., 1995]. When a hypoeutectoid steel is held just above the Ac1, the microstructure partially changes from ferrite plus pearlite to ferrite plus austenite. Some fine cementite particles are retained in the austenite phase. During subsequent slow cooling and holding, these fine cementite particles function as nuclei for spheroidized cementite, mostly on the grain boundaries between the ferrite and austenite. This higher number of retained cementite particles leads to a higher ratio of spheroidized to lamellar cementite [Ochi and Koyasu, 1980] Therefore, retaining the fine cementite particles in the austenite during heating is of prime importance for obtaining spheroidized cementite [Muzak et al., 1995]. Some researchers have further pointed out that the complete dissolution of carbon would generate pearlite below the Ac1 temperature rather than spheroidite [O'Brien and Hosford, 2000].

2.7.2 Subcritical Process

Subcritical annealing occurs when a steel is annealed just below the Ac1 temperature. O'Brien and Hosford [2000] suggested that the fine pearlite produced by extremely rapid cooling after hot rolling should rapidly spheroidized

at the lower critical temperature. The driving force for subcritical spheroidization is reduction of the ferrite-carbide interface area by the transformation of carbide plates to spheres. The mechanism of the transformation is the diffusion of carbon from high-(surface) energy to low-energy sites.

O'Brien and Hosford [2000] revealed that the ductility (reduction of area) of a medium carbon steel was close to its maximum value after one hour of such annealing. Spheroidization was nearly completed within the first two hours, and further time increased the particle size with an associated reduction in their number.

In the present work, subcritical annealing was performed to produce a spheroidized microstructure.

2.8 Development of Non-heat-treated CHQ Steels

Heat treatment, especially the spheroidizing treatment that is often performed on medium carbon and alloy steels prior to cold heading, is a procedure that consumes large amounts of time and energy. Many attempts have been made to eliminate this treatment, including the development of new non-heat-treated steels.

One approach to non-heat-treated CHQ steel is to decrease the carbon content. Koyama et al. [1995] developed SUC80 steels to take the place of the JIS-S45C grade; this was for the manufacture of high strength bolts. Compared with JIS-S45C, the new steels involve a reduction of carbon content from 0.45 wt.% to 0.18-0.22 wt.% and higher contents of Mn and Cr together with additions of V, Ti and B. Research has indicated that these new low carbon steels, combined with a controlled rolling process, have equivalent mechanical

properties and better cold workability than JIS-S45C; plus they eliminate the necessity of a spheroidizing treatment before cold deformation.

Similar research was conducted by Lee et al. [1992]. Low C and high Mn steels were developed for the manufacture of high strength (70kg/mm^2) bolts. These were conventionally made from S45C grade steel, with a heat treatment performed before the cold heading procedure. The composition of the newly developed steels included 0.15-0.20 wt.% C, 1.39-1.60 wt.% Mn, and the addition of Nb or V. Through controlled rolling, low reheating temperature, low rolling temperature, and rapid cooling, a combination of high strength and good ductility was obtained in the as-hot rolled condition.

Microalloyed extra low carbon steels were developed by Tsai et al. [2000]. These normally have very good formability, hence are suitable for cold heading applications. In order to further improve cold headability, the new steels were microalloyed with titanium, niobium and/or boron. Hot-deformation parameters were also investigated. This revealed that cold headability is sensitive to microalloying additions, degree of hot deformation, and cooling rate. The addition of Ti+Nb has a positive influence on the cold headability. When the hot strain is over 20%, the average grain size of the ferrite is significantly refined; therefore the cold headability is increased.

Dual-phase steels are other newly developed CHQ steels that avoid the need for heat treatment. These dual-phase microstructures consist mostly of ferrite and a second phase of bainite, martensite and/or retained austenite. They potentially offer good strength and ductility combinations. Two dual phase steels, DP2 and DP6, with carbon contents of 0.09 wt.% and 0.11 wt.% respectively, have been developed for CHQ. Cold headed bolts made from as-hot rolled DP2 met the strength and hardness requirements for high strength fasteners without any heat treatment before or after cold heading [Wanjara et al., 1999].

Chapter 3

Experiments

The experiments performed in the project included:

- Heat treatment
- Drop weight testing
- Visual inspection
- Optical microscopy (OM) and scanning electron microscopy (SEM) inspection

3.1 Materials

3.1.1 Chemical Composition

As mentioned in Chapter 2, cold headability is affected by the chemical composition of a material. Any deviation in chemical composition may cause a difference in cold headability, thus a single chemical composition was used in this project. The material selected was a medium-carbon grade 1036M CHQ steel, containing 0.34 wt.% carbon, and the chemical composition is listed in Table 3.1. This steel is produced by IVACO for the manufacture of fasteners.

Table 3.1 Chemical composition of 1036M CHQ steel (wt.%)

C	Mn	P	S	Si	Cu
0.34	0.94	0.009	0.015	0.24	0.2
Ni	**Cr**	**Mo**	**Sn**	**Al**	**N**
0.09	0.25	0.30	0.012	0.004	0.0065

3.1.2 Microstructures

In the as-received state, two microstructures were investigated. One was the as-hot rolled state (HR), whose microstructure consisted of lamellar pearlite and ferrite. The other was a basic heat treated state (HT). The heat treatment cycle involved annealing at 745°C for 4 hours, then cooling to 500°C in 5 hours. The microstructure of the HT condition consisted of heat treated pearlite and ferrite. Figure 3.1 shows the microstructures of 1036M steel in the two as-received states.

Figure 3.1 (a) Microstructure of 1036M steel, as-hot rolled state, x2000

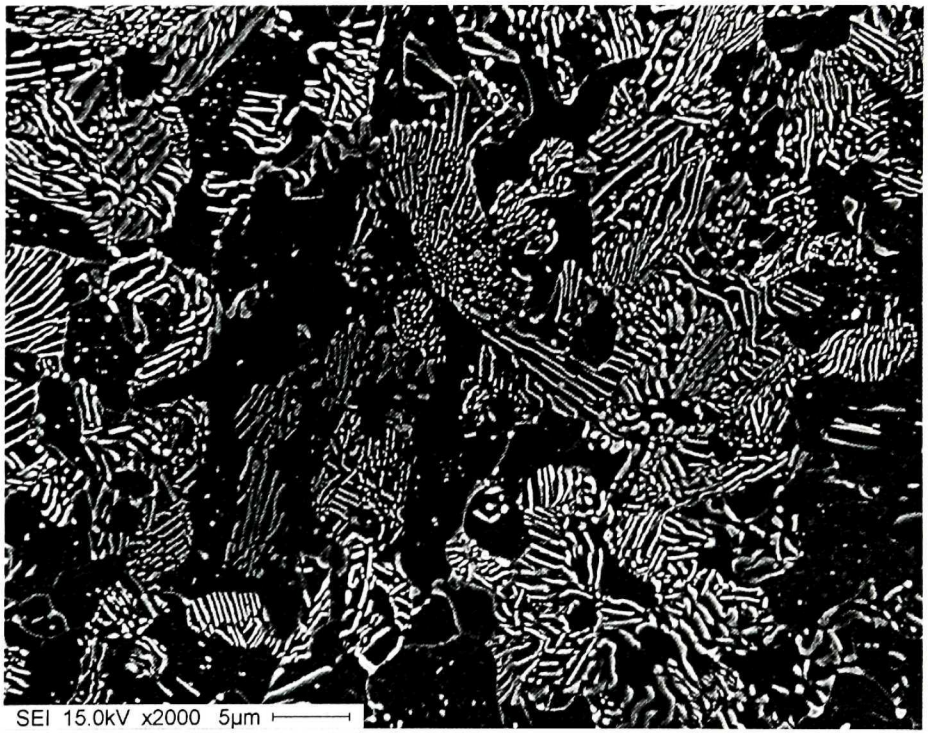

Figure 3.1 (b) Microstructure of 1036M steel, heat treated state (HT), x2000

3.2 Heat Treatment

In addition to the above mentioned conditions, four other microstructures were produced by means of various heat treatments in the lab, so as to determine the effect of microstructure on cold headability. The four microstructures, referred to as Heat Treated I - IV, (HT-I, II, III, IV), were produced as follows:

HT-I: samples were heated to 745°C, held at temperature for 24 hours, then furnace cooled to room temperature.

HT-II, III, IV: samples was heated to 715°C and held at temperature for 24 hours, 4 hours and 1 hour, respectively, then furnace cooled.

The aim of HT-I was to compare the effect on cold headability of microstructures containing lamellar pearlite with that containing completely spheroidized cementite. HT-II, III and IV were used to compare the effect of different degrees of spheroidizing.

These heat treatment cycles are summarized in Table 3.2.

Table 3.2 Heat treatments to produce different microstructures

Heat Treated I **(HT-I)**	Annealed at 745°C for 24 hours
Heat Treated II **(HT-II)**	Annealed at 715°C for 24 hours
Heat Treated III **(HT-III)**	Annealed at 715°C for 4 hours
Heat Treated IV **(HT-IV)**	Annealed at 715°C for 1 hour

The furnace used was an electric muffle type, with no protective atmosphere applied during the heat treatment.

3.3 Drop Weight Test (DWT)

Drop weight tests were performed to measure the cold headability of the tested materials.

3.3.1 Drop Weight Tower

The DWT machine consisted of a tower that guided weight plates dropping down onto a die set and stop blocks. The weights were changeable to generate various impact loads. A cylindrical sample was held vertically in the die set on a central column that was fixed to the base of the machine. The die was set so that the impact force was forwarded to workpiece. Two pneumatic cylinders, fixed to the base, worked as shock absorbers to avoid secondary impact caused by rebounding of the weight. The die set assembly is shown in Figure 3.2.

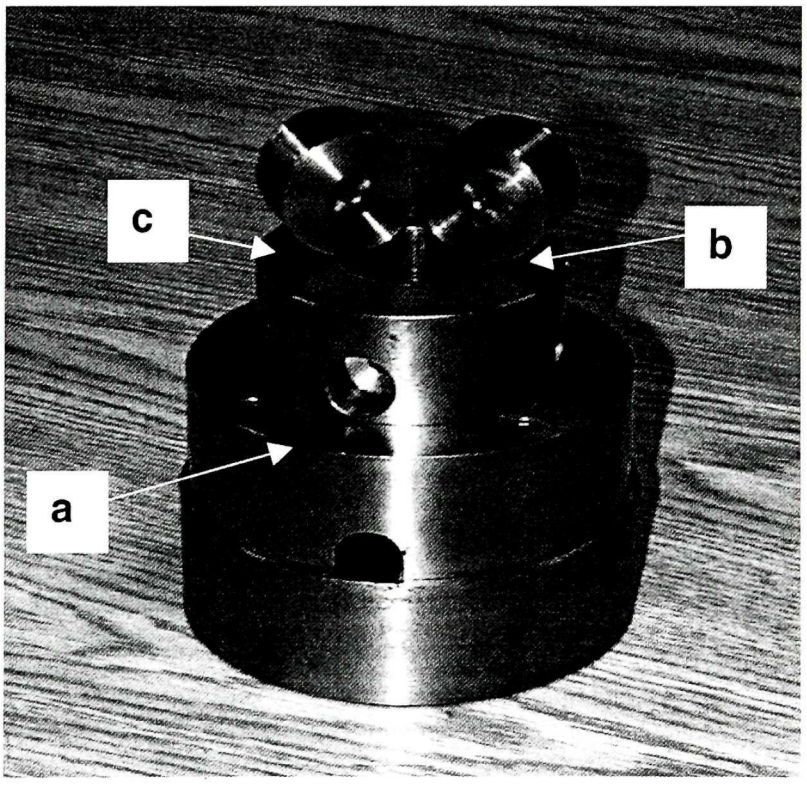

Figure 3.2 Die set assembly of DWT; (a) die sleeve; (b) lower die, (c) upper die

3.3.2 Specimen Preparation

As explained in Chapter 2, cold headability is affected by the surface condition of the material. In order to avoid any influence of surface condition in the current investigation, all DWT samples were smoothed by machining.

The DWT samples were of a cylindrical shape with a diameter of 5.2mm. An aspect ratio of 1.24 was chosen for all microstructures, whilst 1.0 and 1.6 were also tested for the HR and HT materials. The resulting sample heights were 8.24, 7 and 10 mm respectively.

3.3.3 Drop Weight Test

The DWT can be controlled by changing either the drop weight or the drop height. Varying the drop height causes a change in strain rate; therefore, in this work, the height was kept constant and varying weights were used in ascending order. In the tower, the maximum drop weight was limited by the length of the two thread bars, which penetrated through the weight plates and tied them together. Thus when this limit was reached, a new drop height was taken and kept constant, whilst the drop weight was varied again in an ascending manner.

Previous work revealed that a drop height of 1.5 m is suitable for fracturing a similar medium carbon (1038) steel [Nickoletopoulos, 2001]. Therefore, the primary drop height was set at 1.5 m and the drop weight was varied in increments of 2.3kg from 11.35kg until the sample cracked. Once this rough weight limit was established, the weight was decreased at intervals of 0.6 kg to determine the minimum weight at which a crack was generated. Three samples were tested for each condition.

3.4 Fracture Evaluation

Cold headability is measured in terms of the surface strain at which the first crack is initiated; thus observing and measuring cracks is the key for its determination. However, this is a subjective measurement; there is no industry standard available to evaluate the surface quality of cold headed parts. In this work, the surface observations on the DWT's samples were divided into three classes: no crack, ghost line crack, and open crack, as illustrated in Figure 3.4. A stereomicroscope was employed to inspect these surface cracks and the presence of a ghost line crack at a magnification of x 25 was used to classify the failure of a tested sample. The surface strain of a deformed sample was measured as shown in Figure 3.3.

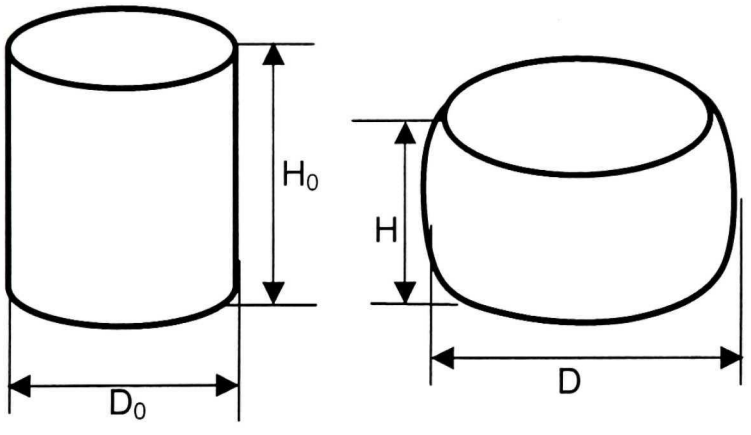

Axial strain:

$$\varepsilon_z = \ln \frac{H}{H_0}$$

Circumferential strain:

$$\varepsilon_\theta = \ln \frac{w}{w_0} = \ln \frac{D}{D_0}$$

Figure 3.3 Measurement of surface strain

A JEOL JSM-840A scanning electron microscope was used to observe the cracks and fracture surfaces of tested samples. Energy Dispersive Spectrum (EDS) analysis was employed to qualitatively determine the chemical composition of particles observed on these fracture surfaces.

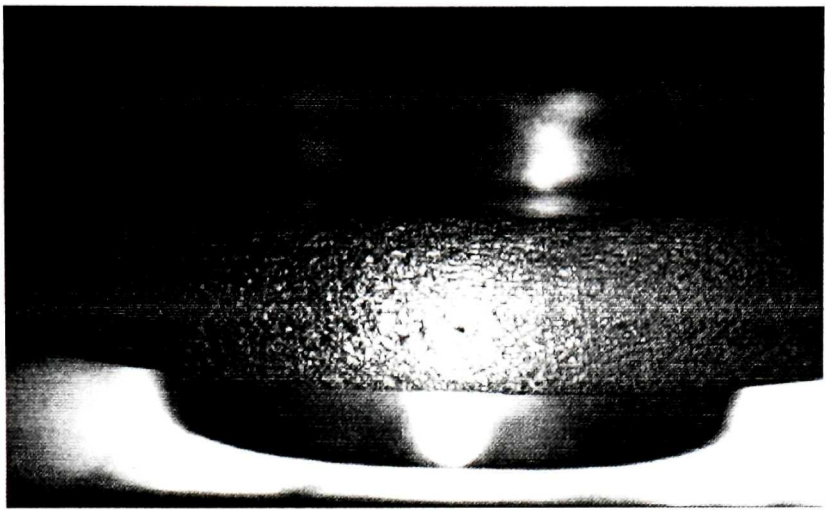

(a) Surface with no cracks

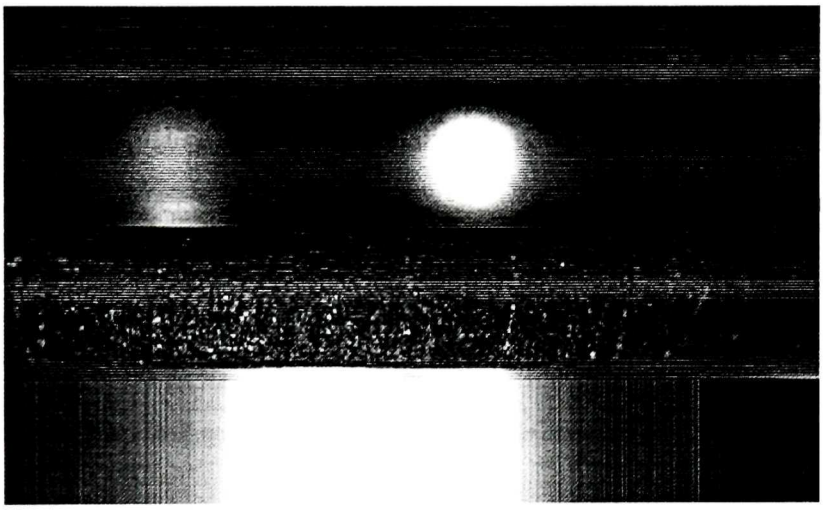

(b) Ghost line cracks

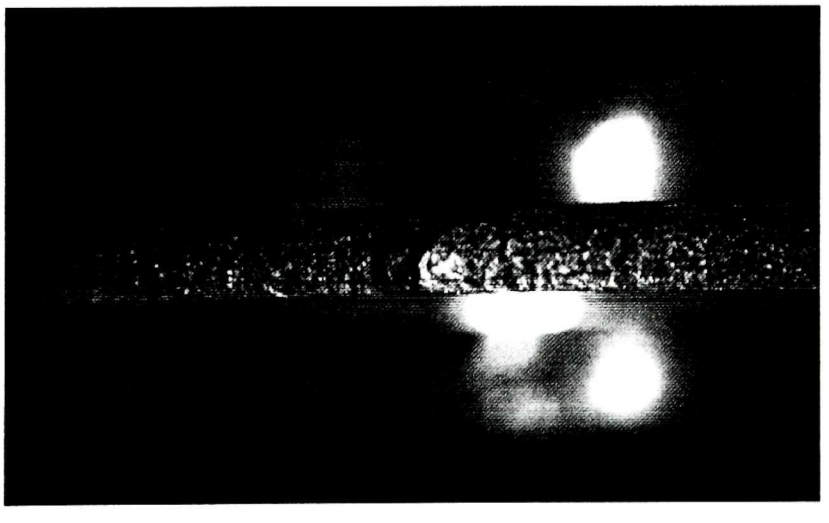

(c) Open crack

Figure 3.4 Illustration of three crack classes in DWT specimens

Chapter 4

Results

4.1 Heat Treatment

Heat treatments were performed according to the cycles listed in Table 3.1 to produce four additional microstructures, as shown in Figures 4.1 – 4.4.

HT-I, annealed at 745°C for 24 hours, then furnace cooled, consisted of equiaxed pearlite and ferrite. This is because the hot rolled pearlite was transformed into austenite above the Ac1 temperature (approximately 720 °C), and transformed to pearlite again during cooling.

HT-II, annealed at 715°C for 24 hours, then furnace cooled, consisted of spheroidized cementite distributed in a ferrite matrix. Because this temperature was below the Ac1, no phase transformation occurred during heating, holding and cooling. However, due to the elevated temperature, lamellar cementite in the pearlite was converted into spheroidal cementite.

HT-III and HT-IV, annealed at 715°C for four hours and one hour respectively, had microstructures similar to that of HT-II, but were characterized by different degrees of spheroidization.

Figure 4.1 Microstructure of HT-I, x2000

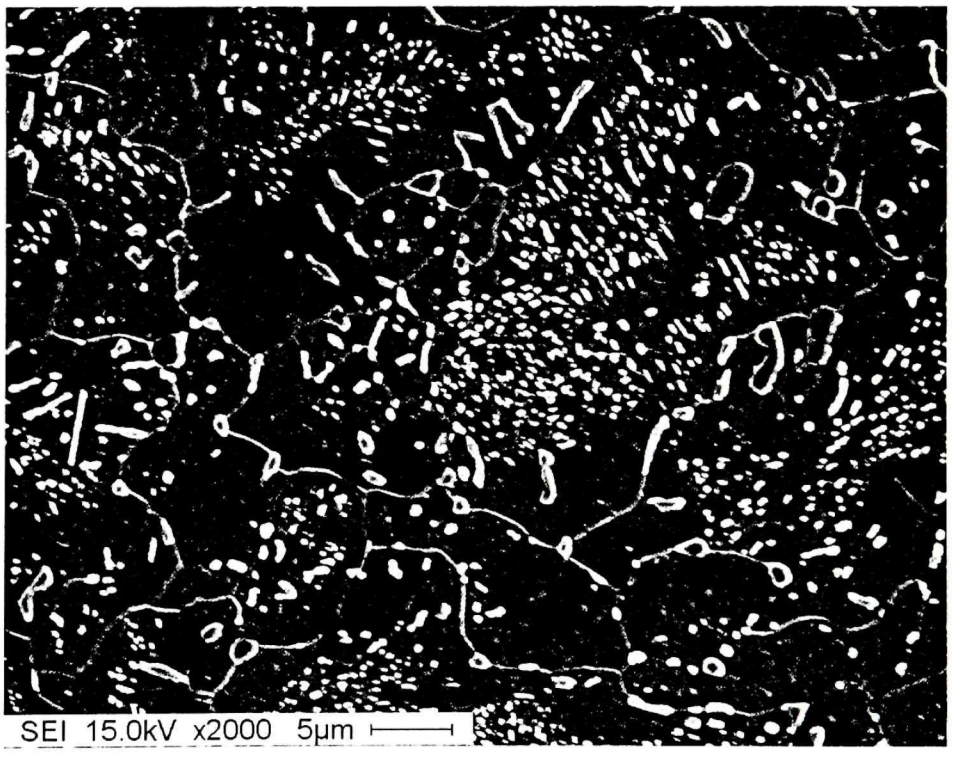

Figure 4.2 Microstructure of HT-II, x2000

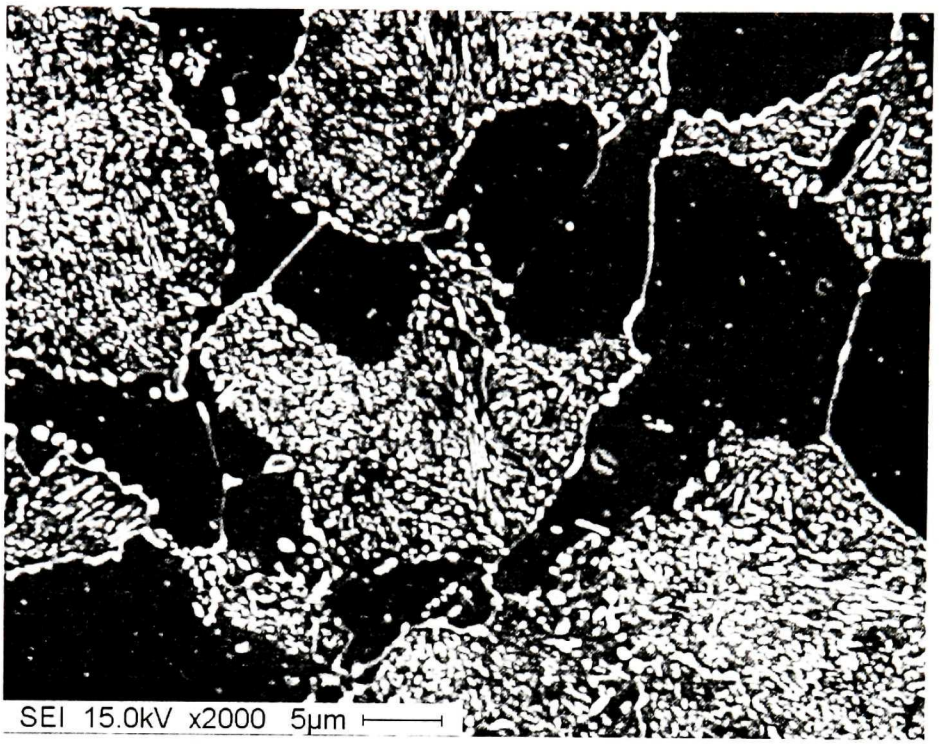

Figure 4.3 Microstructure of HT-III, x2000

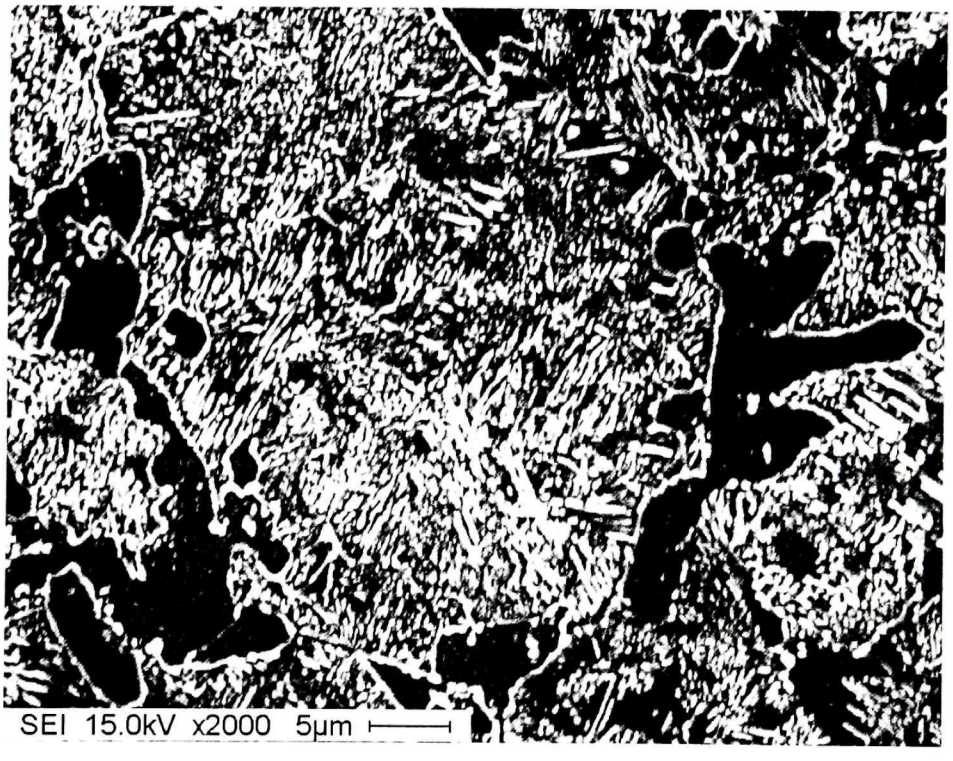

Figure 4.4 Microstructure of HT-IV, x2000

4.2 Drop Weight Test Results

DWT testing was performed on the 6 materials with specimen aspect ratios of 1.24, so that all the microstructures could be compared at an identical aspect ratio. HR and HT were additionally tested at aspect ratios of 1.0 and 1.6.

The dimensions of the samples were measured before and after the DWT's, so that the axial and circumferential strains could be calculated. The surfaces of the tested samples were carefully inspected under a magnification of x25 and the minimum strain at which the first crack initiated was taken as the fracture strain. Table 4.1 lists the DWT fracture strains for all six microstructures at an aspect ratio of 1.24. These are expressed using lower and upper limits; the lower limit is defined as the strain at which the first crack occurred, whereas the upper limit is the maximum strain at which no crack was found. No cracks were found below the lower limit and all samples were cracked above the upper limit.

HR, the as-hot rolled material, had the lowest axial and circumferential fracture strains. Compared with HR, there was no significant improvement with the HT microstructure. However, HT-II had the best cold headability, with the largest axial and circumferential strains among the six microstructures. HT-I and HT-III had similar intermediate values. Comparing HR and HT-II, the lower limits of the axial and circumferential strains of HT-II were 21% and 17% higher than those of HR. The differences between the fracture strains are due to the different microstructures of the tested materials.

Table 4.2 indicates the fracture strains of HR and HT for aspect ratios of 1, 1.24 and 1.6. The fracture strains increased with increasing aspect ratio. This is in agreement with the theory of fracture limit diagrams.

Table 4.1 DWT fracture strains for various microstructures

	Aspect Ratio	Axial Strain	Circumferential Strain
HR	1.24	1.52 – 1.70	0.77 – 0.88
HT	1.24	1.59 -1.63	0.82 - 0.84
HT-I	1.24	1.75 -1.89	0.89 - 0.93
HT-II	1.24	1.84 -1.95	0.9 - 0.99
HT-III	1.24	1.76 -1.81	0.88 - 0.93
HT-IV	1.24	1.58 -1.84	0.8 - 0.94

Table 4.2 DWT fracture strains for different aspect ratios

	Aspect Ratio	Axial Strain	Circumferential Strain
HR	1	1.4-1.59	0.71-0.79
HR	1.24	1.52 – 1.70	0.77 – 0.88
HR	1.6	1.76-1.85	0.85-0.92
HT	1	1.5-1.58	0.75-0.83
HT	1.24	1.59 -1.63	0.82 - 0.84
HT	1.6	1.78-1.8	0.88-0.91

The samples cracked by DWT were carefully examined. Most cracks were of a longitudinal type, whilst some equiaxed small fractures and widely opened fractures were also found. Figure 4.5 shows typical cracks and fractures that were observed in the DWT samples. Figure 4.5 (a) depicts a longitudinal crack that is narrow and extends along the length of the sample. Figure 4.5 (b) is a small "equiaxed" fracture on the barrel of the sample; whilst Figure 4.5 (c) is a widely opened fracture, which penetrates through the entire length of the deformed sample. The equiaxed fracture can be seen to be made up of two perpendicular shear fractures.

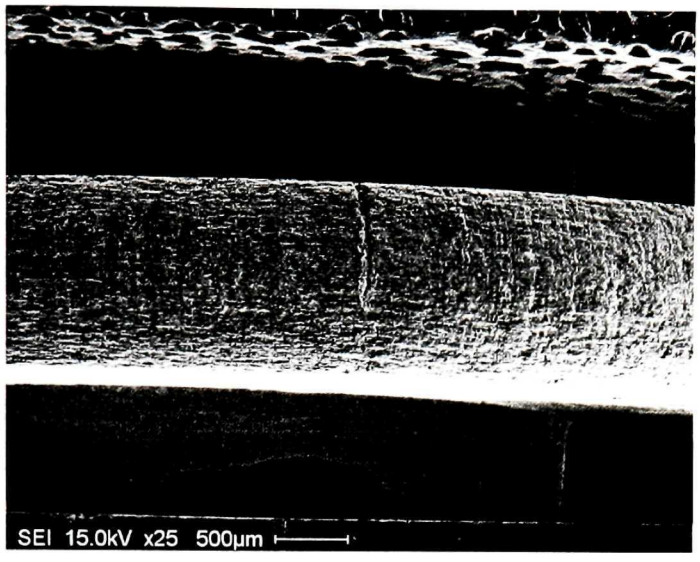

(a) longitudinal crack

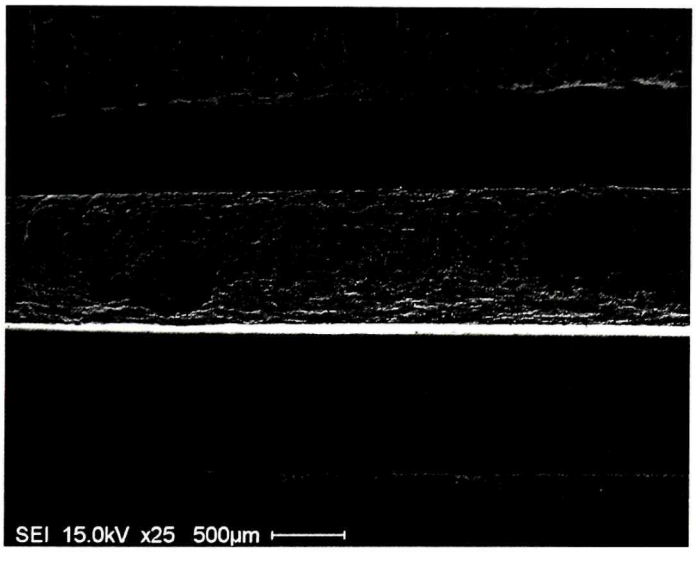

(b) small equiaxed fracture

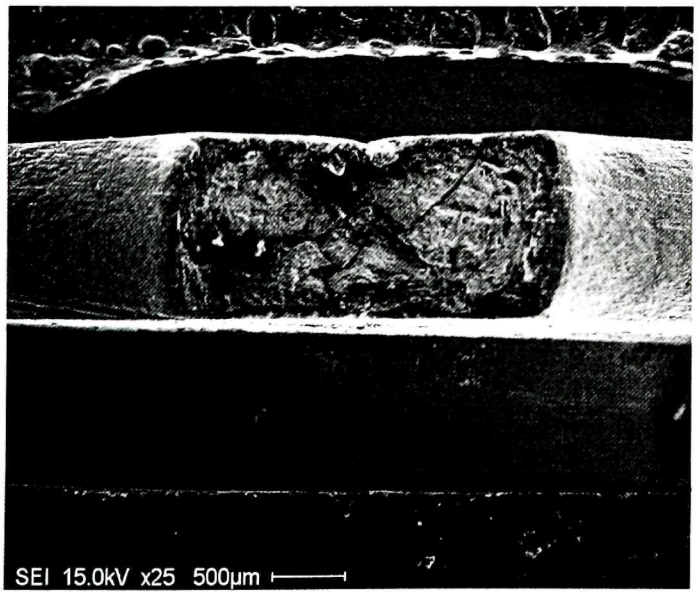

(c) widely opened fracture. Mag. x25

Figure 4.5 Fractures on DWT samples

Chapter 5

Discussion

5.1 Drop Weight Test Results

The objective of the present work was to evaluate the cold headability associated with different microstructures by means of measuring the axial and circumferential strains at which a crack is initiated. As discussed in Chapter 2, it is widely agreed that commonly used test methods in the fastener industry, such as tensile and upset testing, are not able to assess cold headability satisfactorily, [Olsson et al., 1986; Muzak et al., 1995]. The main problem with these traditional techniques is that they do not correspond to the conditions of cold heading deformation in terms of strain rate, stress state and friction. In the present work, the DWT was employed to simulate the cold heading process.

The DWT is designed to deform and crack a cylindrical sample, held in a pair of sleeve-guided dies, under an impact load caused by a dropping weight. The impact energy (E) is a function of the mass (M) and velocity (V),

$$E = \frac{1}{2} MV^2 \qquad (6)$$

The impact velocity is a function of the drop height (h),

$$V = \sqrt{2gh} \tag{7}$$

Therefore, the impact energy is adjustable by varying the drop weight and/or drop height.

The DWT is capable of applying deformations at very high strain rates. During impact, the strain rate decreases from the initial strain rate, corresponding to the impact velocity, to zero. Using a 1.5 m drop height, the initial strain rate can be as high as $630s^{-1}$ for an aspect ratio of 1.6 and $820s^{-1}$ for an aspect ratio of 1.3 [Nickoletopoulos, 2001].

The die set of the present DWT is designed in the form of a sleeve guide, with a pocket on each die to stabilize the specimen. The upper die moves along the die sleeve, so that the specimen is deformed exactly along its axis.

When a cylindrical specimen is deformed in uniaxial compression, the strain is initially uniformly distributed along the axis. Nevertheless, stress concentrations develop between the matrix and inclusions or second phase particles. When the circumferential stress on the equatorial free surface of the cylindrical specimen becomes increasingly tensile, due to the occurrence of barreling, a state of tensile plastic instability can be reached. The high stress concentrations at inclusions or second phase particles within this highly strained region rupture the bonds with the matrix or alternatively crack particles, thus nucleating voids [Thomason, 1969].

Many researchers have employed "naked eye" observations to detect the presence of cracks on the barrel surface. However, Nickoletopoulos [2001] used a stereomicroscope at x25 magnification for such determinations. This latter method is more stringent than the "naked eye" technique, which may result in an

overestimate of the fracture strain. In the present work, the stereo microscopy method was again employed. The observation of a ghost line at x25 magnification was used to define the failure of a sample.

DWT was performed on all six microstructures; all samples had the same chemical composition. The test results, which were listed in Chapter 4, are presented in a different format in Table 5.1 and Figures 5.1 and 5.2.

Table 5.1 Minimum impact energy to cause cracking (aspect ratio: 1.24)

	Drop Weight (kg)	Drop Height (m)	Impact Energy (J)	Axial Strain
HR	28.8	1.5	423	1.52
HT	24.1	1.5	354	1.59
HT-I	29.9	1.9	567	1.75
HT-II	28.8	2.1	592	1.84
HT-III	25.8	1.9	480	1.76
HT-IV	29.9	1.5	440	1.58

Table 5.1 lists the values of impact energy that caused initial (ghost line) cracking in the tested materials. From the table, it can be seen that the HT microstructure has the lowest impact fracture energy, but the fracture strain is not significantly greater than that for the HR material. This indicates that the HT heat treatment only softened the material, without significantly improving its formability. HT-II had the highest impact energy among the six tested materials, corresponding

to an axial strain of 1.84. This indicates that the HT-II heat treatment best improved the cold headability. HT-I and HT-III led to similar fracture strains, but the HT-I impact energy was 16% higher than that of HT-III. This indicates that a spheroidized microstructure has a lower deformation resistance than a microstructure containing lamellar pearlite. The HT-IV fracture strain was close to that of HT, whose impact energy was a little higher than that of HR.

As explained in Chapter 4, lower and upper limits were used to define the range of strains attainable without fracture. The strains below the lower limit were deemed to be well within the safe zone, whilst strains above the upper limit were definitely in the fracture zone. Strains between the lower and upper limits were deemed to be in the danger zone. No cracks were observed in the safe zone, cracks were always found in the fracture zone, whilst cracks may or may not have developed in the danger zone. It is evident that the larger the safe zone, the better the cold headability of the material.

Figure 5.1 shows that the as-hot rolled microstructure, which contains large amounts of lamellar pearlite, has the lowest amount of allowable strain, whereas HT-II has the largest safe zone amongst the six tested materials. HT and HT-IV were similar; both were more formable than HR. HT-I and HT-III were also similar over the extent of the safe zone.

Figure 5.2 displays the DWT results for the HR and HT samples tested using different aspect ratios. In general, the fracture strain increased with increasing aspect ratio. The greater the aspect ratio in a heading operation, the lower the stress concentration effect at the free surface [Thomason, 1969B] and hence the greater the cold headability. This is in agreement with the theory of workability limit diagrams. Therefore, comparisons of the cold headability should be conducted on specimens of similar aspect ratio.

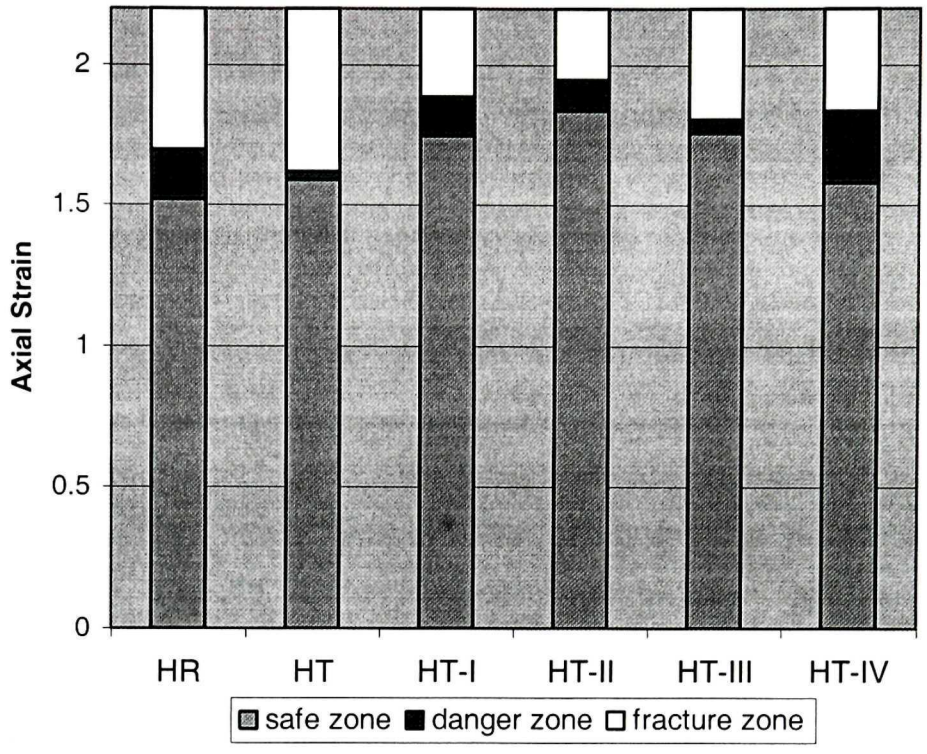

Figure 5.1 DWT fracture results for all microstructures at an aspect ratio of 1.24

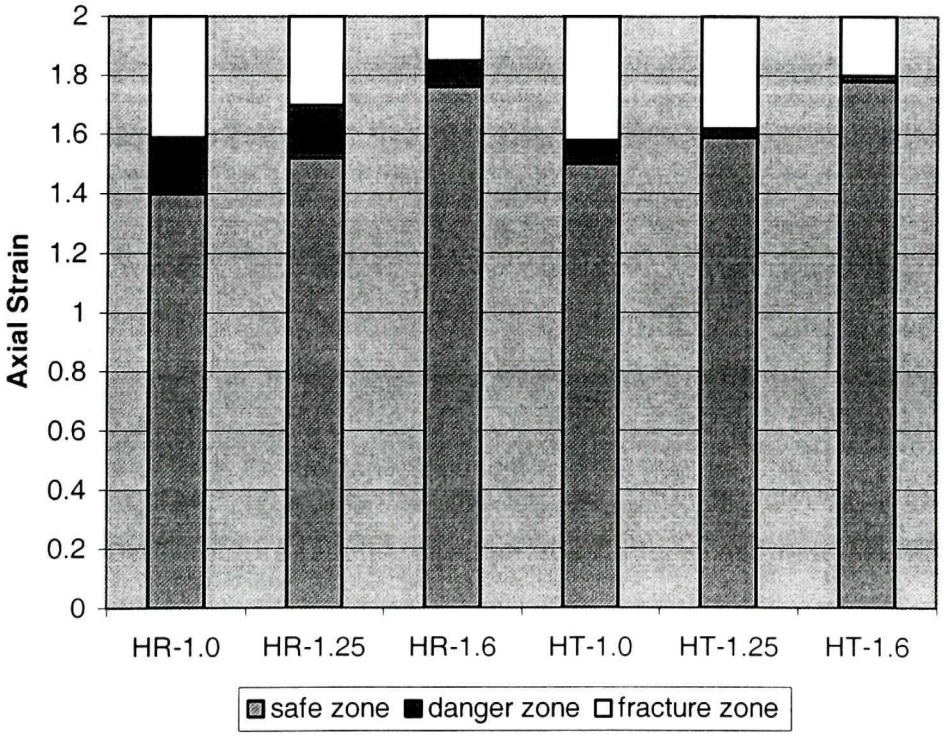

Figure 5.2 DWT fracture results for the HR and HT microstructures at aspect ratios of 1.0, 1.24 and 1.6

5.2 Effect of Microstructure

As mentioned in previous chapters, cold headability depends on chemical composition, surface condition and microstructure. The present work was focused on the effect of microstructure. All the material used in this work was of the same chemical composition, containing 0.34 wt.% carbon. The surfaces of the samples were smoothed by machining. Hence it can be concluded that all the variations between test results were due to microstructural differences.

The as-hot rolled (HR) microstructure consisted of ferrite and pearlite. These constituents formed during phase transformation on the STELMOR conveyor. Due to the fast cooling on the conveyor, relatively high pearlite fractions were present in this microstructure.

The HT material had been prepared by heating to and holding at 745° C for 4 hours, then cooling to 500° C in 5 hours. The microstructure contained ferrite and pearlite; the latter was mostly of lamellar form and was spheroidized in a few areas. The pearlite fraction was lower in the HT microstructure than in the HR material. As the annealing temperature was in the ferrite-austenite dual phase region, phase transformation from pearlite to austenite occurred at 745° C and the long holding time at this temperature also resulted in the formation of pro-eutectoid ferrite. During subsequent cooling, the remaining austenite transformed into pearlite. Due to the relatively slow cooling rate, some of the pearlite was spheroidized during this cooling period.

In order to confirm the above analysis, a heat treatment test was conducted. A sample was heated to 745° C and held at this temperature for 4 hours, then quenched to room temperature. Ferrite and martensite were found in the microstructure of this sample, as shown in Figure 5.3.

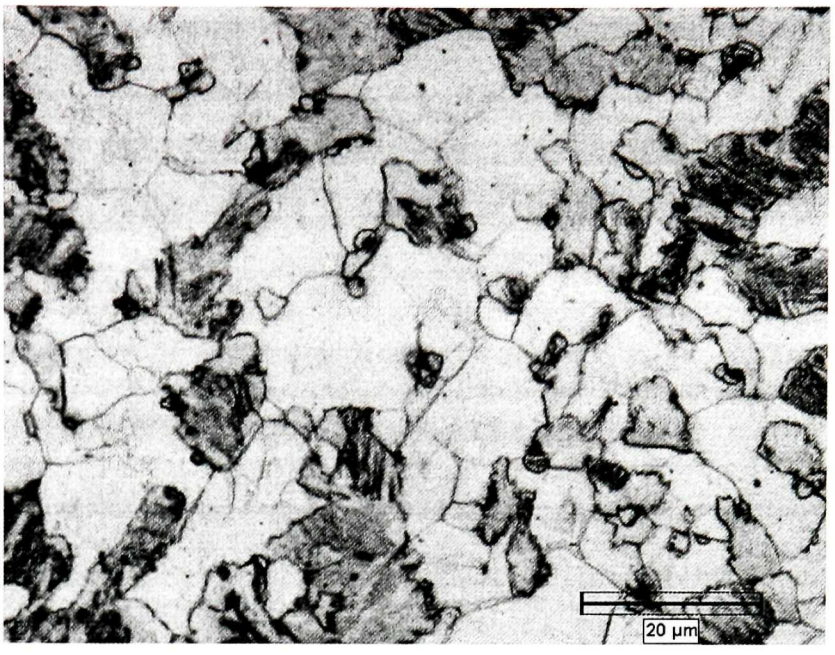

Figure 5.3 Microstructure of annealed and quenched base steel, consisting of ferrite and martensite, X 1000

The HT-I microstructure was developed by annealing at 745° C for 24 hours. The microstructure consisted of equiaxed ferrite and lamellar pearlite, formed during cooling. The pearlite fraction in HT-I was much lower than in HR.

HT-II, HT-III and HT-IV were developed by annealing at 715° C for 24 hours, 4 hours and 1 hour, respectively. Because of the long holding time close to the Ac_1 temperature, the pearlite in HT-II was completely spheroidized. Partial spheroidization occurred in the HT-III sample, whereas only small regions of the HT-IV microstructure were spheroidized.

The tested materials consisted of a two-phase mixture of ferrite and pearlite or spheroidized cementite. The volume fraction of each phase in the mixture influences the strength and formability of the material. In general, the hard phase of such a mixture contributes to the material's strength and hardness, whereas the soft phase contributes ductility and toughness [Gurland, 1988].

The volume fraction of pearlite in each material was measured by means of an optical microscope using image analysis (Clemex) software. HR had a volume fraction of 78% pearlite, HT-IV was close to HR with 75%, and HT had 63%. HT-II had the lowest pearlite fraction with an average of 43%, while HT-I and HT-III contained 48% and 52%, respectively. The measured results are listed in Table 5.2.

Table 5.2 Volume fraction of pearlite (%)

HR	HT	HT-I	HT-II	HT-III	HT-IV
78	63	48	43	52	75

Pearlite in carbon steel is the hard phase and contributes to its hardness. Spheroidized cementite also works as a second phase. The effect of the second phase is to decrease ductility and impact toughness [Pickering, 1980], Therefore, decreasing the pearlite fraction will improve the cold headability.

Goods and Brown [1979] have given the relationship between the critical strain to nucleate a void and the volume fraction of second phase particles:

$$\varepsilon_{cri} = 1.7\frac{r}{b}\left(\frac{\sigma_1 - \sigma_H - \sigma_0}{\mu}\right)^2\left(1 + 3f_v + \frac{f_v^{\frac{1}{2}}}{1.8}\right)^{-2} \qquad (8)$$

ε_{cri} - critical strain to nucleate a void

b - Burgers vector

f_v - particle volume fraction

r - particle radius

σ_I - interfacial strength

σ_0 - Orowan stress

σ_H - hydrostatic tension

μ - shear modulus

It is evident from this relationship that increasing the second phase volume fraction (f_v) results in a decrease in the critical strain required to nucleate a void (ε_{cri}).

Figure 5.4 shows the relationship between the fracture strain and the volume fraction of pearlite. With decreasing pearlite fraction, the fracture strains (axial and circumferential) increase. This is because the interfacial areas of the two phases are the regions of high stress concentration. Void nucleation occurs at the sites of high stress concentration [Van Stone at al., 1985]. Raising the volume fraction of pearlite, therefore, results in an increase in the density of void nucleation sites; hence it deteriorates the cold headability.

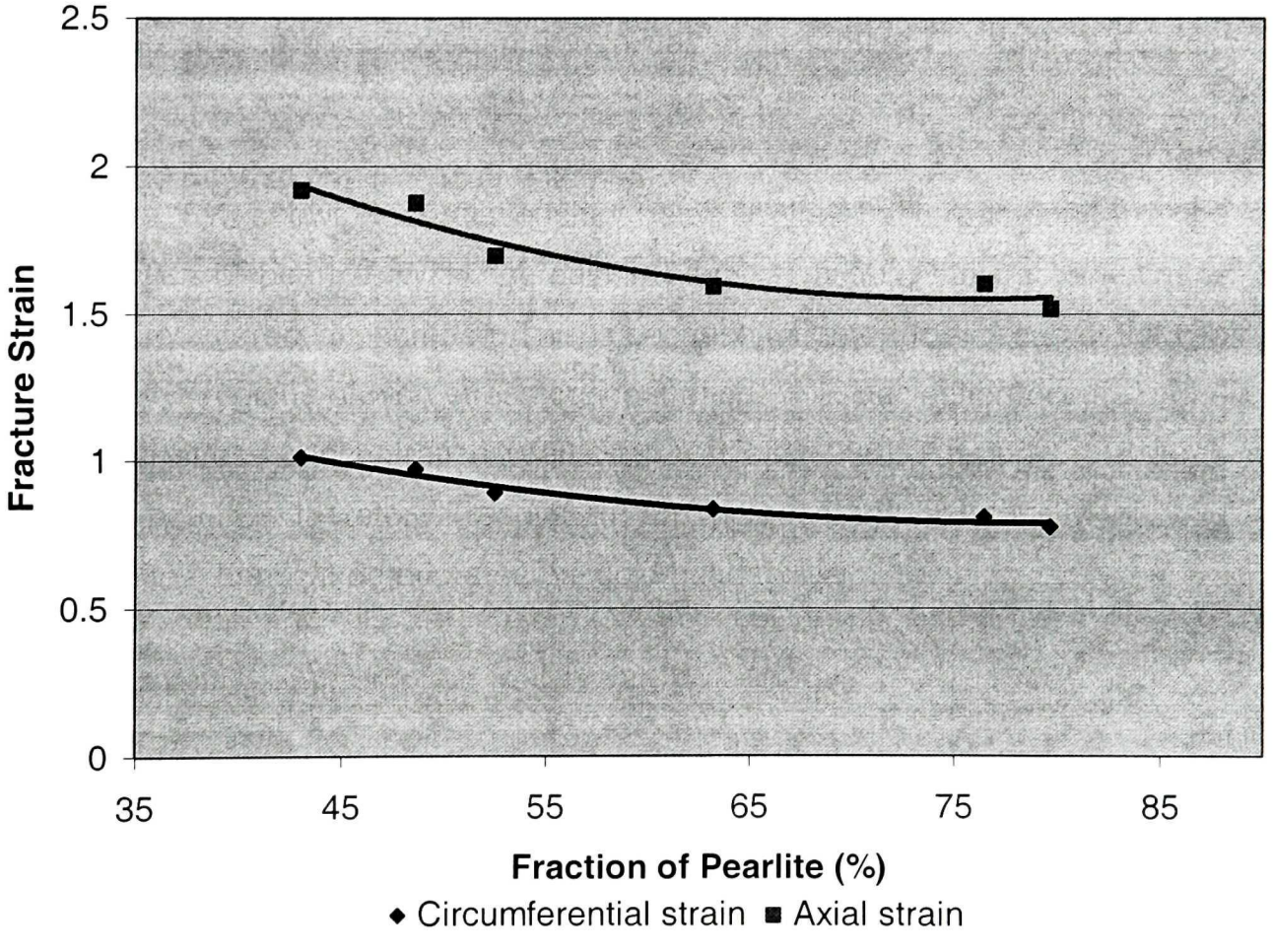

Figure 5.4 Fracture strain vs. volume fraction of pearlite

The stress concentration at the interface results from the difference in mechanical properties between the two phases. As ferrite is the soft phase, it contributes to the material's ductility; pearlite is the hard phase and contributes to the hardness. The difference in ductility between the two phases leads to high stress concentrations at their interfaces during deformation. When the concentration exceeds a critical value, voids nucleate on these interfaces or at second phase particles. The smaller the difference in ductility between the two phases, the better the cold headability.

In order to determine the difference in strength and hence ductility between the two phases, microhardness analysis was used. The microhardness (Vickers microhardness at a load of 50 grams) of ferrite and pearlite colonies in each material was measured at multiple points on each phase for an undeformed sample, so that the average microhardness and in this way the disparity between the ferrite and pearlite colonies was obtained.

Figure 5.5 shows the average microhardnesses and the differences between the phases for all the tested materials. HR, whose microstructure was formed on the STELMOR conveyor, had the highest values in the pearlite and ferrite, as well as the largest disparity between them amongst all six tested materials. After heat treatment, the microhardnesses of both the pearlite colonies and the ferrite decreased to different degrees, as did the disparity values.

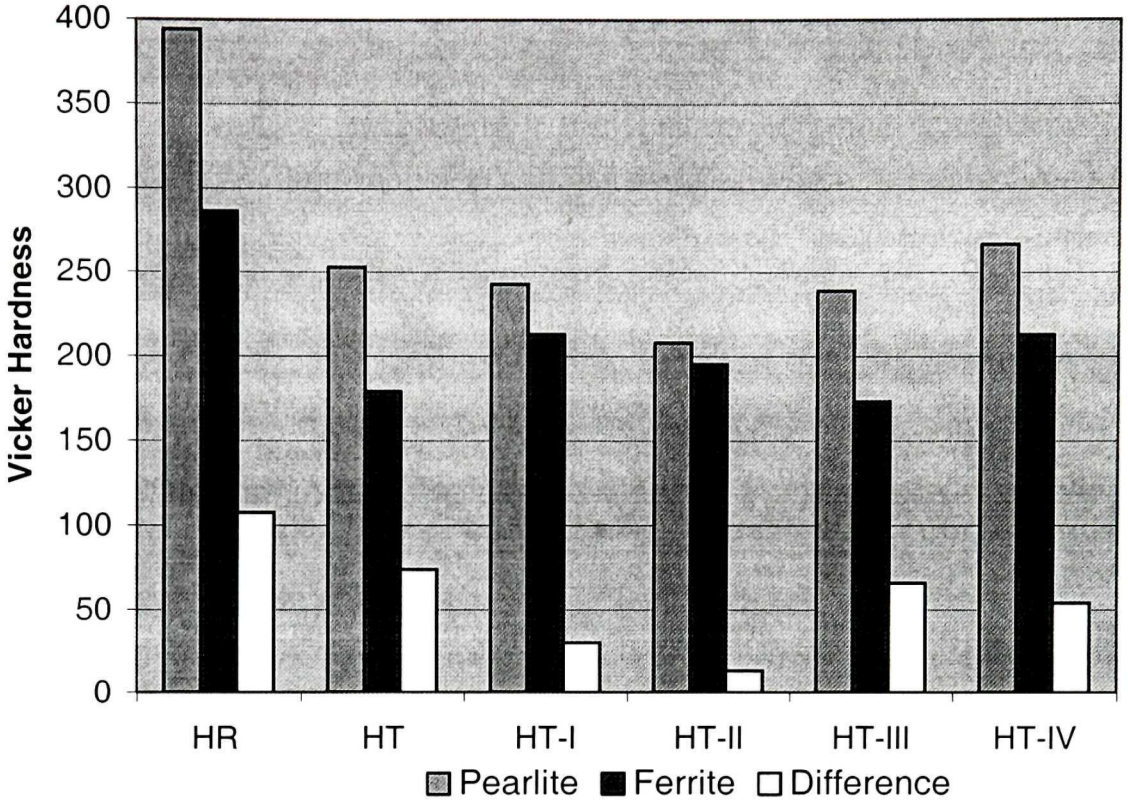

Figure 5.5 Differences between undeformed pearlite and ferrite microhardnesses

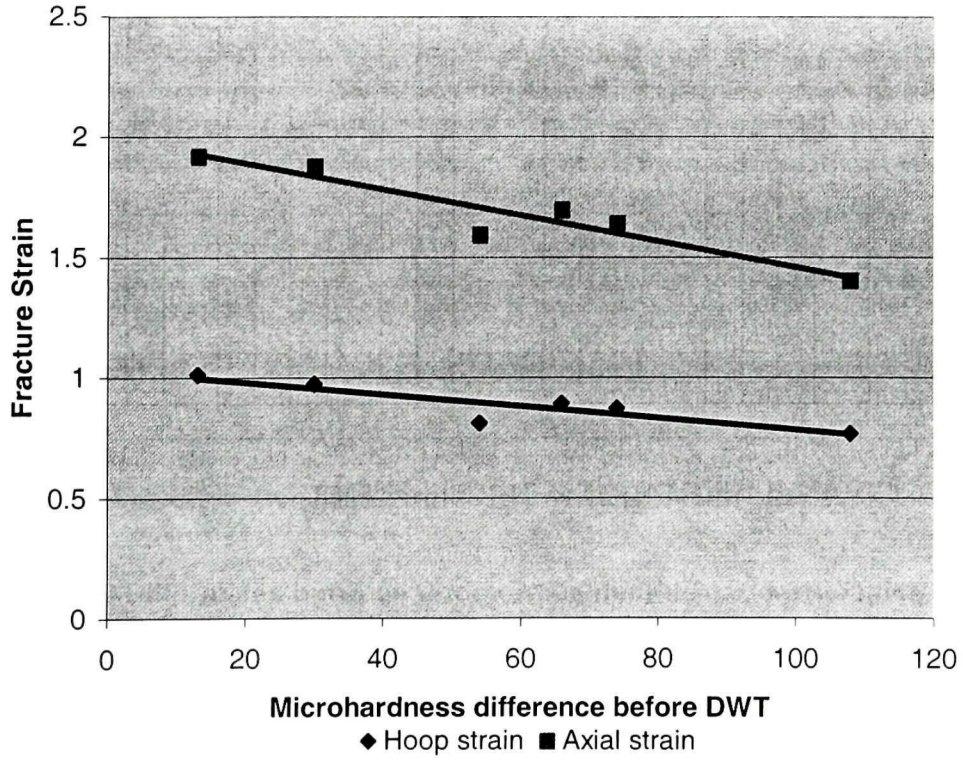

Figure 5.6 Relationship between microhardness difference and fracture strain

The HT-II material had the smallest microhardness difference between phases. Note, however, that some uncertainty may be involved in the microhardness values, because the dimensions of some spheroidal cementite particles were so small that the test indenter probably covered some adjacent ferrite in certain cases.

Figure 5.6 displays the relationship between the microhardness difference before DWT and the fracture strain. The fracture strain decreased with an increase in the microhardness disparity. It is evident that higher disparity values result in higher stress concentrations at the phase interfaces and therefore to an increase in the probability of nucleating microvoids and fractures.

The sizes and shapes of second phase particles are also factors that affect the characteristics of fracturing. Fisher and Gurland [1981] reported that voids in spheroidized carbon steel were generally associated with particles whose dimensions were of greater than average size and that they rarely formed at very small particles. Non-equiaxed or irregularly shaped cementite particles were often subject to internal fractures. Particles situated at ferrite grain boundaries were favored sites for the nucleation of voids.

The fracture stress of a second phase particle may be calculated using an energy balance approach. It has been assumed that when the elastic energy stored in a second phase particle exceeds the surface energy for a newly formed void, fracture can occur at the particle. The relationship between the critical stress for particle cracking (σ_c) and particle size (d) was provided by Van Stone [1985].

$$\sigma_c = \left(\frac{6\gamma E}{q^2 d} \right)^{\frac{1}{2}} \qquad (9)$$

E - particle Young's modulus γ - surface energy of particle

q – particle stress concentration factor

Trufiakov [1992] revealed that the fracture toughness of two-phase steels was determined by the volume fraction and particle size of the second phase component. He gave the relationship between the crack resistance and the second phase fraction and size as the following:

$$\delta = \frac{A}{V_{sp}\sqrt{h_{sp}}} \qquad (10)$$

δ - crack resistance

V_{sp} - volume fraction of second phase

h_{sp} - size of second phase

A - coefficient

From the above discussion, it is evident that increasing the dimensions of the second phase will decrease the critical stress required to cause particle cracking, as well as the crack resistance and so deteriorate the formability.

The HT-II, III and IV materials, which were annealed at the same temperature but for different holding times, differed in the distribution of the carbides present; this is shown in Figure 5.7. The pearlite was spheroidized to different degrees in these microstructures. Here the "spheroidization ratio" is defined as the ratio of the number of spheroidal cementite particles to the total number of cementite particles including those of lamellar form [Das et al., 2002].

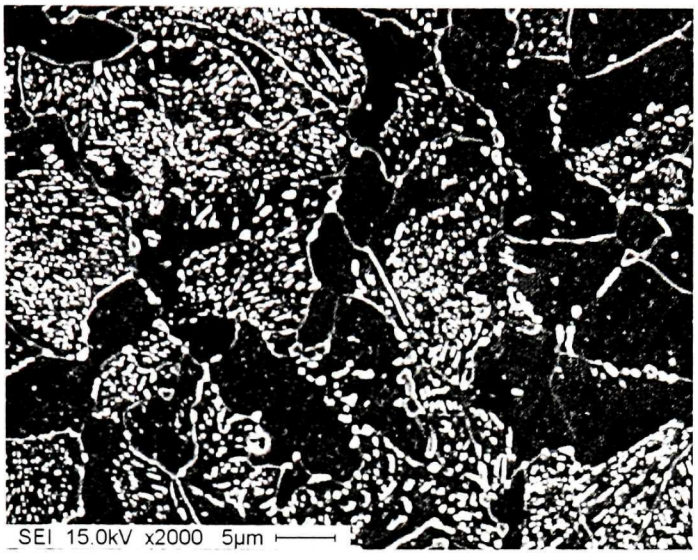

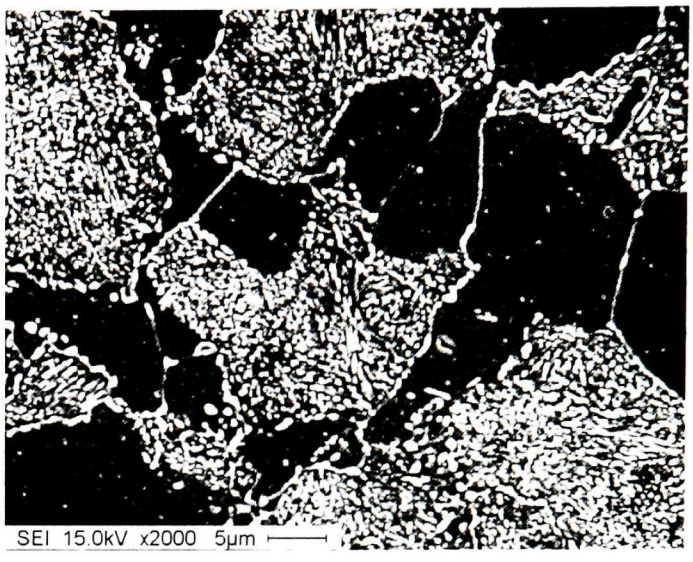

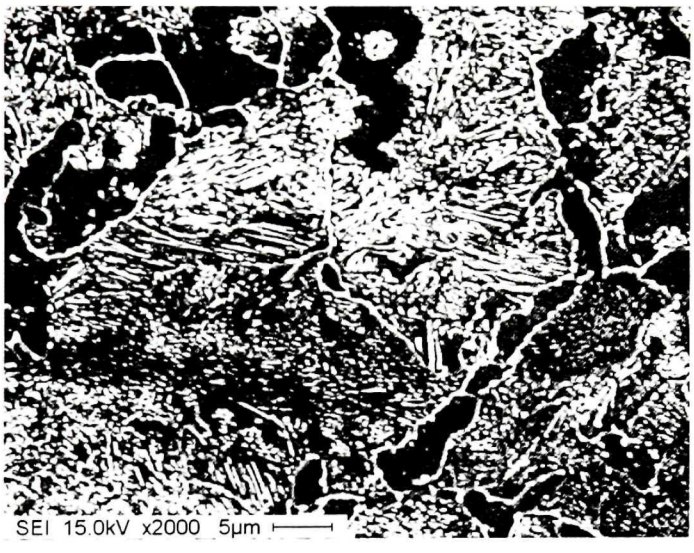

Figure 5.7 SEM micrographs of (a) HT-II, (b) HT-III, (c) HT-IV, x2000

Several researchers [Chattopadhyay and Sellars, 1977; Das et al., 2002] have employed the "aspect ratio" of the cementite to evaluate the degree of spheroidization. The aspect ratio is defined as the length ratio of the long axis to the short axis of a cementite particle. When this ratio is less than a critical value, the particle is deemed to be spheroidized. Chattopadhyay and Sellars chose 5 as the criterion, whilst Das chose 2.

Such a quantitative analysis of spheroidization was not carried out in the present work. Nevertheless, it is qualitatively evident that the aspect ratios of

almost all the cementite particles in the HT-II and III materials are less than 5, as shown in Figures 5.7 (a) and (b), which indicates complete or nearly complete spheroidization. The aspect ratios of most of the cementite particles are greater than 5 in the HT-IV material, Figure 5.7 (c). Because the second phase aspect ratio was the highest, the headability of the HT-IV material was the lowest of the four steels heat treated in the laboratory.

5.3 Crack Analysis

The purpose of DWT is to ascertain the crack resistance by deforming a cylindrical sample to cracking. In addition to the fracture strain, the crack profile and orientation were also observed. From the profile and orientation of a crack, the fracture mechanism can be determined qualitatively.

Nickoletopoulos [2001] concluded that longitudinal cracks are due to exhaustion of the matrix ductility, whilst shear cracks are the result of localization induced by local softening and plastic instability. Other research has revealed that longitudinal cracks can be caused by the presence of surface defects on cold heading rod, so that the plastic limit of the material is reached more quickly. [Thomason, 1968; Muzak et al., 1995].

In the present work, all the samples tested by DWT exhibited longitudinal cracking at the point of initiation. Figure 5.8 shows the first crack on one sample of each of the tested materials. Most of the DWT samples exhibited a narrow longitudinal crack on the barrel surface, even when the strain was moderately high. Some of the "longitudinal" cracks were seen to consist of segments of shear cracks, e.g. Figure 5.8 e.

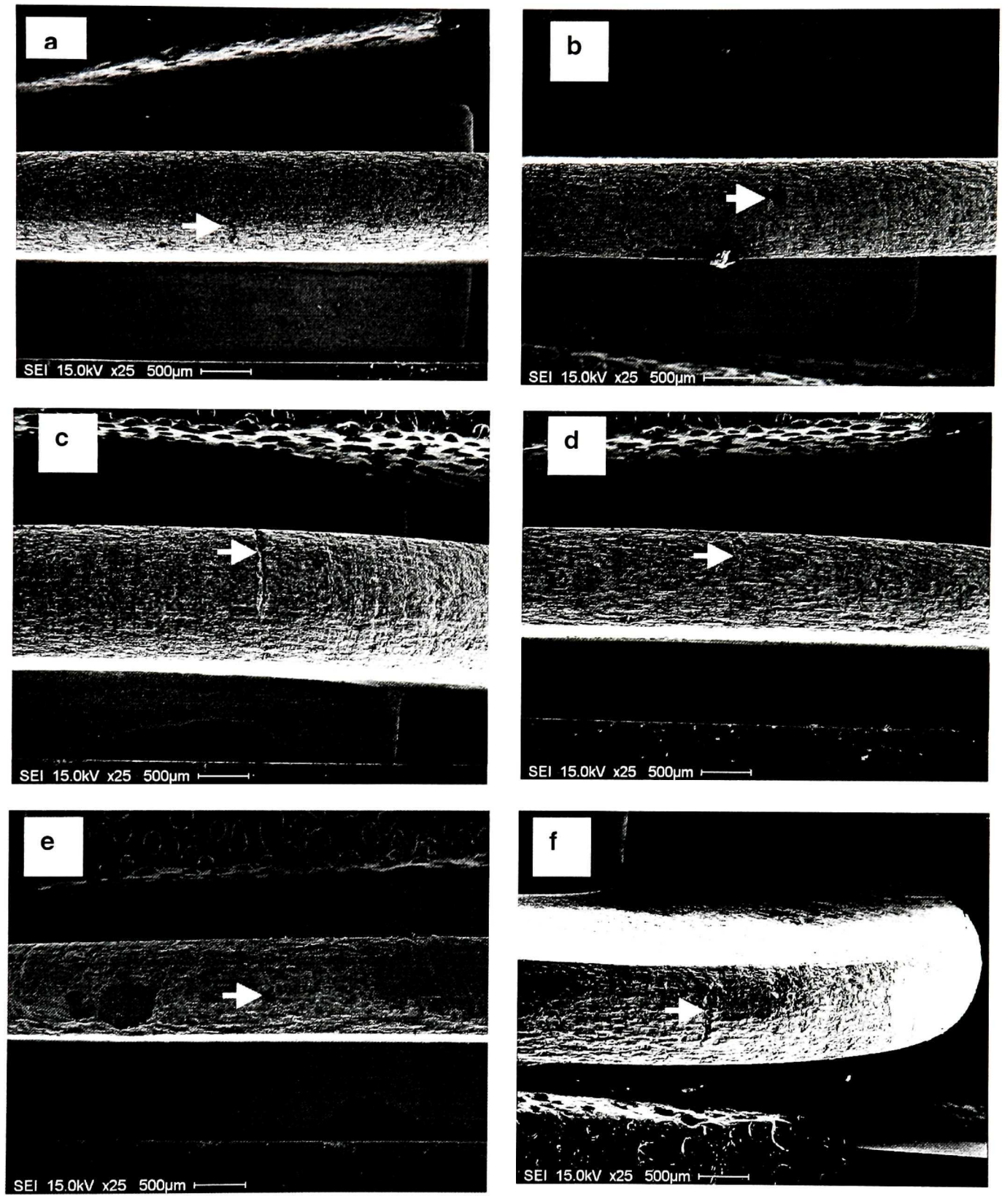

Figure 5.8 Cracks on DWT samples, (a) HR, (b) HT, (c) HT-I, (d) HT-II, (e) HT-III, (f) HT-IV, X25

However, widely opened fractures occurred on some samples of the HR, HT and HT-IV materials, even at moderate strains. These all contained non-equiaxed pearlite. No widely opened cracks were found in the HT-II and III grades. Figure 5.9 illustrates a widely opened fracture on an HR sample with an aspect ratio of 1.24, an axial strain of 1.8 and a circumferential strain of 0.9. The fracture edges are widely separated on the barrel surface and several internal cracks of a shear nature extend from the root of the fracture along the different directions. Figure 5.10 shows a widely opened fracture on another HR sample with an aspect ratio of 1.24; here the axial and circumferential strains were 1.68 and 0.84, respectively. The morphology of the fracture is similar to that of the previous HR sample and again the shear character of the internal cracks is evident.

A widely opened crack of the HT material is shown in Figure 5.11. The aspect ratio of the sample was again 1.24 and the measured axial and circumferential strains were 1.69 and 0.86, respectively. Compared with the two previous HR samples, the HT fracture is narrow and short. This fracture does not completely traverse the barrel surface. Figure 5.12 displays a widely opened fracture on the surface of an HT-I sample whose strains were 1.89 and 0.93, respectively. This fracture was widely opened on the barrel surface and a zigzag (shear) crack can be seen to characterize the root of the fracture.

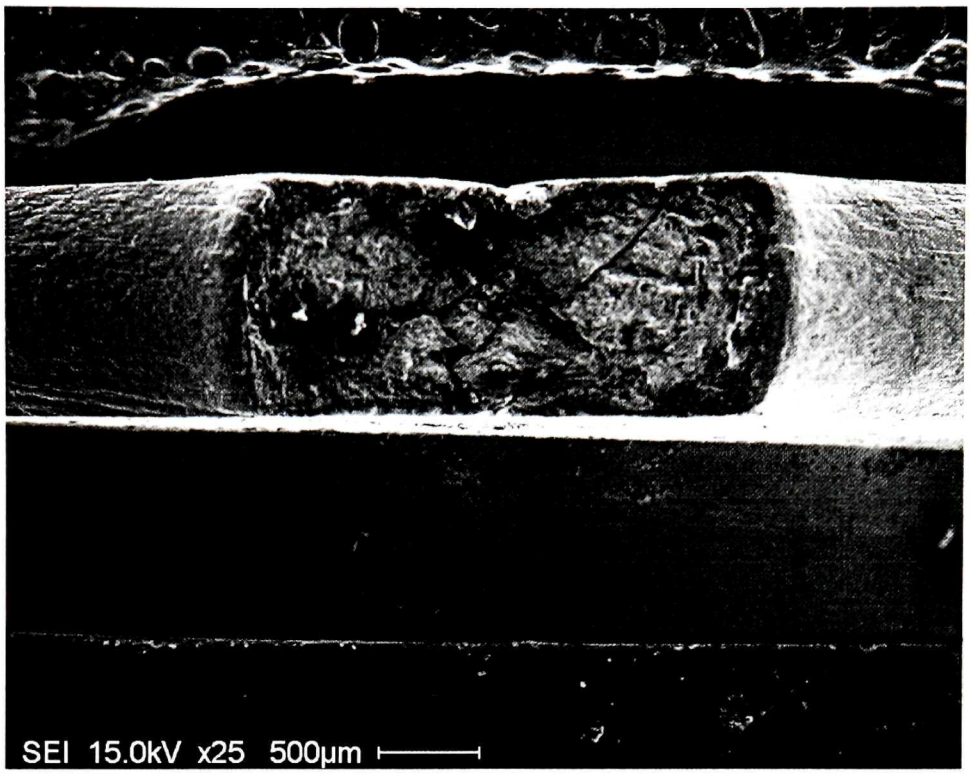

Figure 5.9 Widely opened fracture on HR sample, aspect ratio 1.24, axial strain 1.8 circumferential strain 0.9, x25

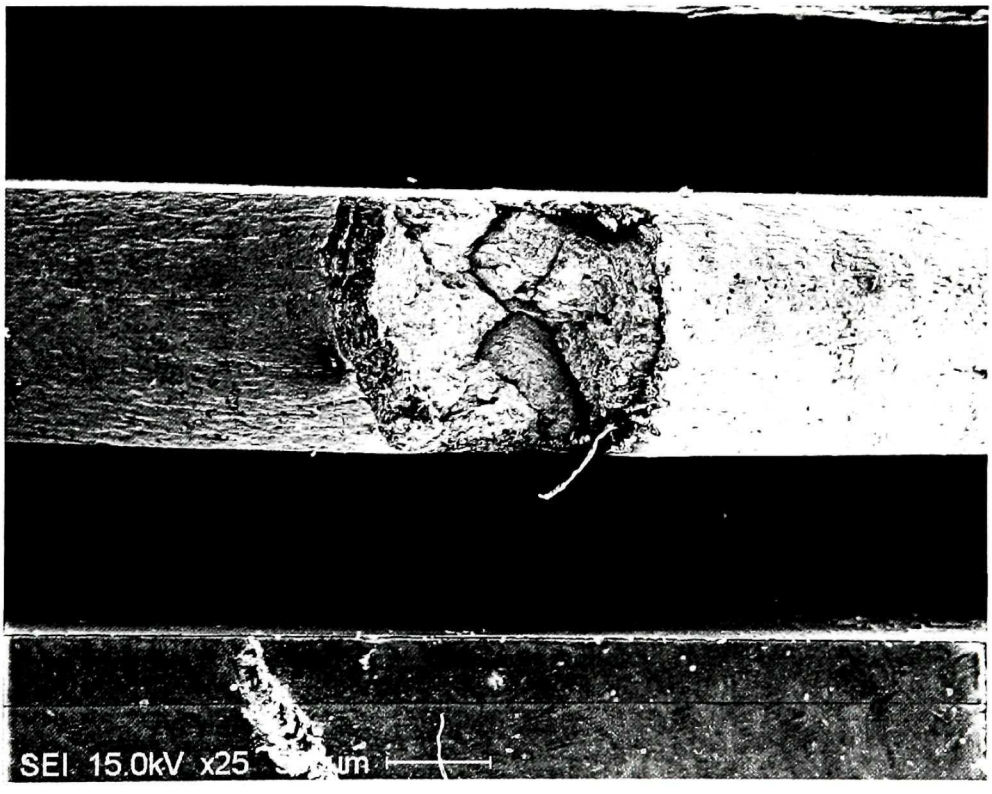

Figure 5.10 Widely opened crack on HR sample, aspect ratio 1.24, axial strain 1.68, circumferential strain 0.84, x25

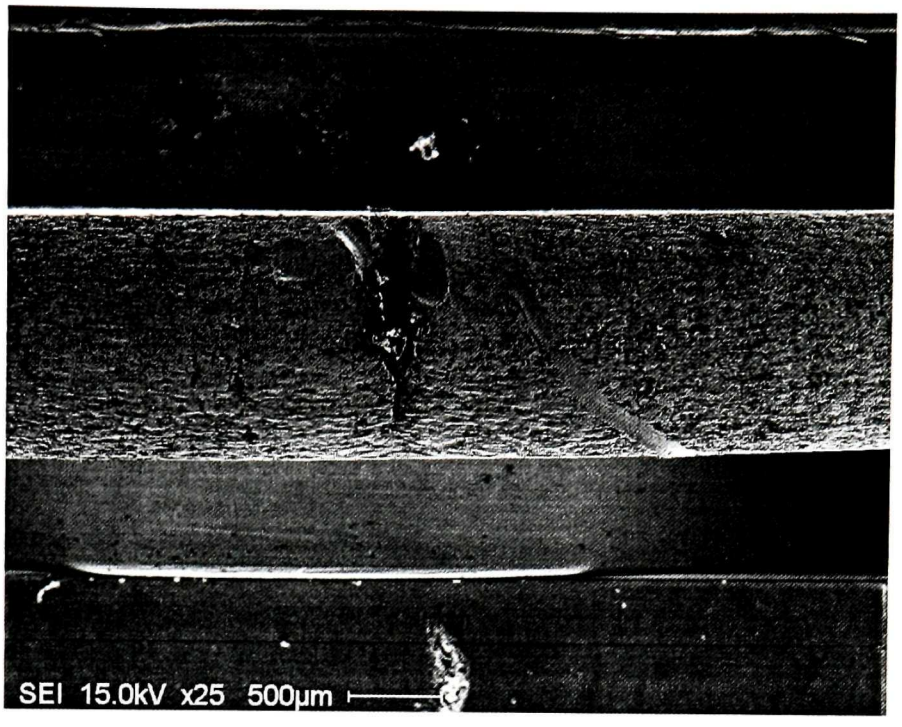

Figure 5.11 Widely opened crack on HT sample, aspect ratio 1.24, axial strain 1.69, circumferential strain 0.86, x25

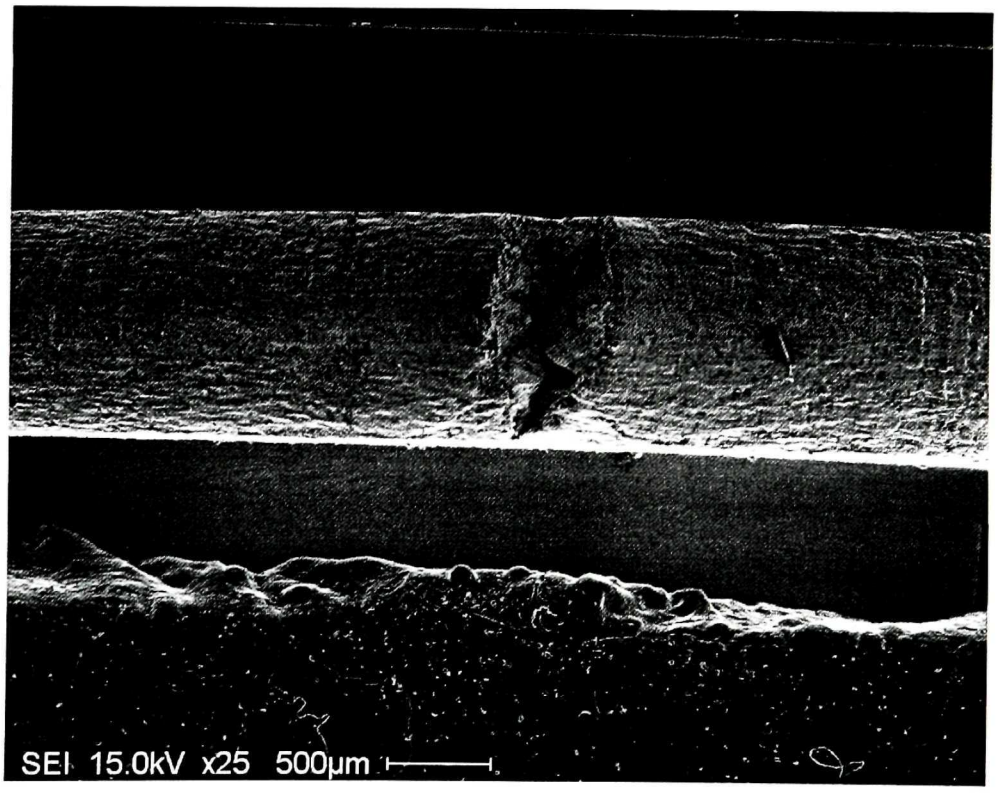

Figure 5.12 Widely opened fracture on HT-I sample, aspect ratio 1.24, axial strain 1.89, circumferential strain 0.93, x25

SEM observations were also made. The fracture surfaces were seen to exhibit large amounts of voidal depressions separated by ridges that are remnants of ligaments. The dimples, which were distributed randomly, were mainly equiaxed and of different sizes. Figure 5.13 illustrates some of the dimples on the fracture surface of an HR sample. Some particles are observed to be lodged in the bases of the dimples and most of these are elongated.

The presence of the dimples on the fracture surface indicates that the failures of the DWT samples took place by ductile fracture controlled by a microvoid coalescence mechanism. The microvoids were initiated at the second phase particles or at interfaces between the matrix and the particles as a result of the stress concentrations discussed above [Van Stone et al., 1985]. These second phase particles can be inclusions, particles of spheroidal cementite, or an entire pearlite colony, where the latter consists of alternate cementite and ferrite platelets [Metal Handbook, MCIC, 1975]. The dimples were formed as a result of the growth and coalescence of the microvoids.

Second phase particles play important roles in fracture development. Particles found at the bottom of dimples, such as those in Figure 5.13, are responsible for the initiation of voids. Figure 5.14 shows a spheroidal carbide particle on the fracture surface of an HR sample. Figure 5.15 displays the particles on another area of the fractured sample of Figure 5.13. Most of the particles are elongated and some are broken into pieces. Figure 5.16 presents a particle on the fracture surface of an HT-I sample.

Energy Dispersive Spectroscopy (EDS) was employed to determine the particle compositions qualitatively. Most of the particles shown in Figure 5.13 were carbides, whilst a few particles were manganese sulphides. Figure 5.17 is the X-ray spectrum of the particle identified by an arrow in Figure 5.13. The spectrum revealed that the particle, which is located in a dimple, was an MnS particle. MnS

inclusions were also found on the fracture surface (particle A in Figure 5.15). This particle was elongated and broke during deformation.

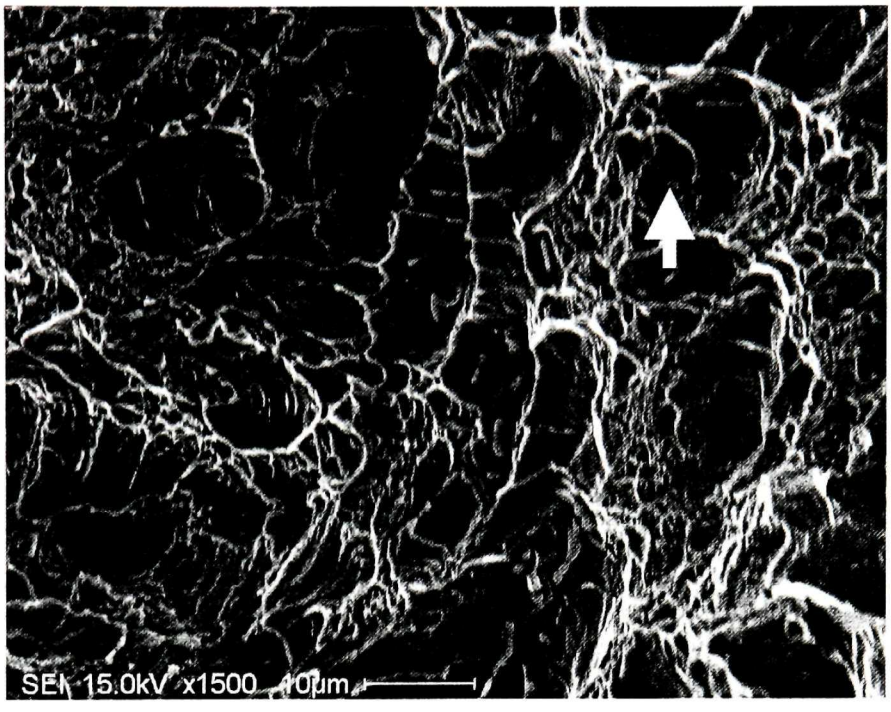

Figure 5.13 Dimples on fracture surface of an HR sample, x1500

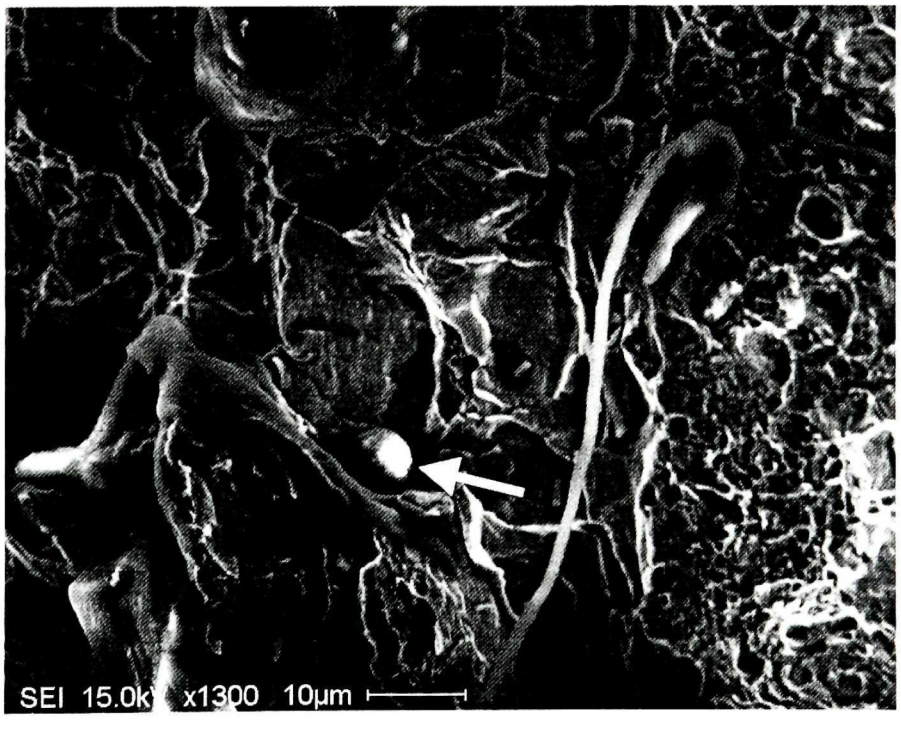

Figure 5.14 A spheroidal carbide particle on the fracture surface of an HR sample, x1300

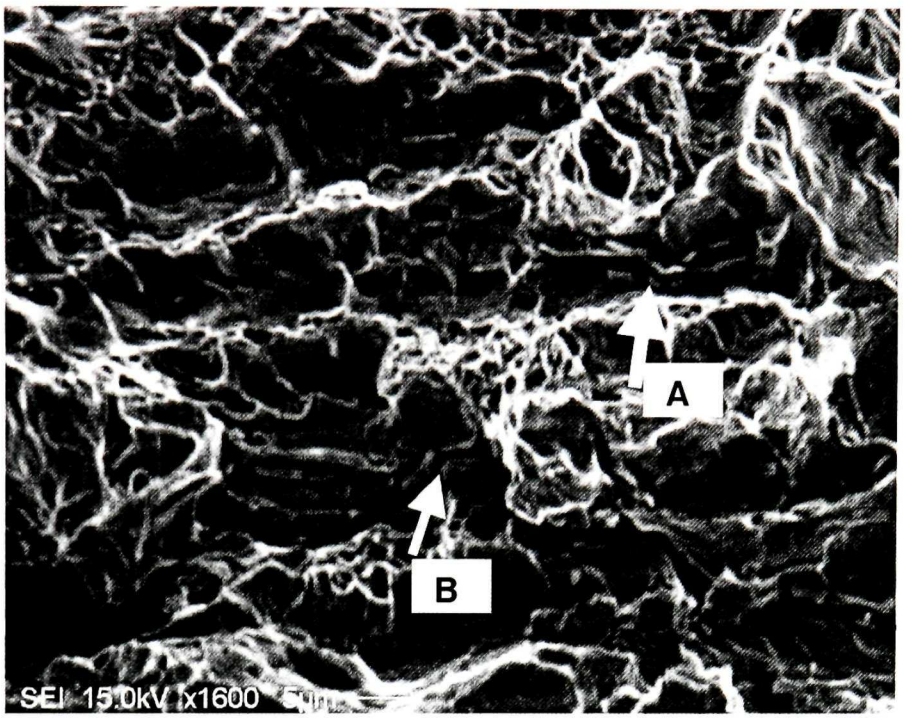

Figure 5.15 Dimples and inclusions on fracture surface of an HR material, x1600

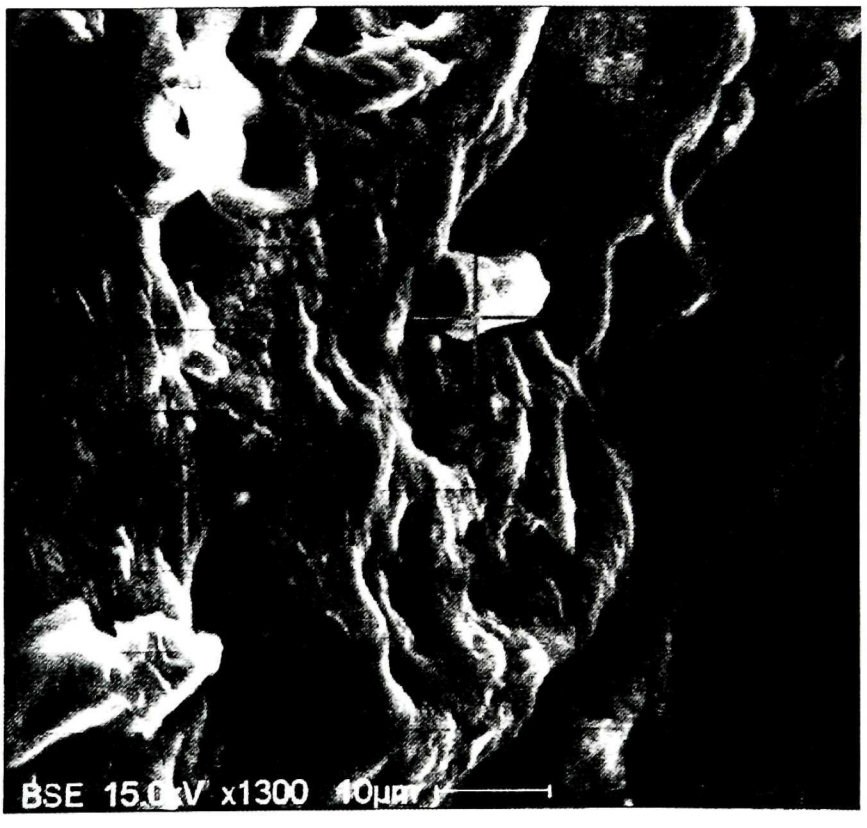

Figure 5.16 Carbide particle on the fracture surface of an HT-I sample, x1300

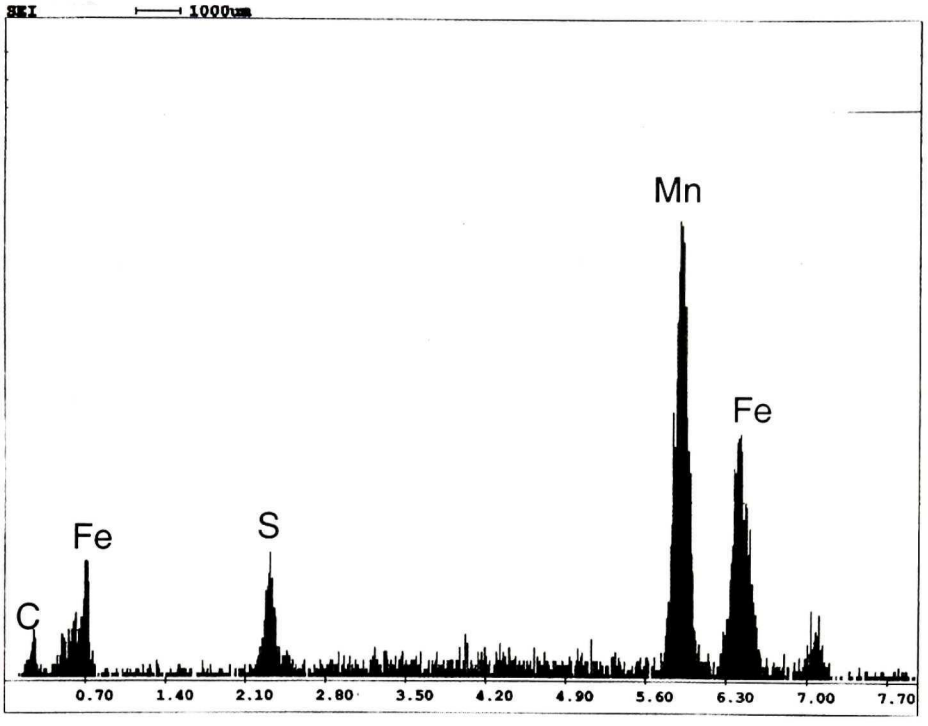

Figure 5.17 X-ray spectrum analysis of arrowed particle in Figure 5.13

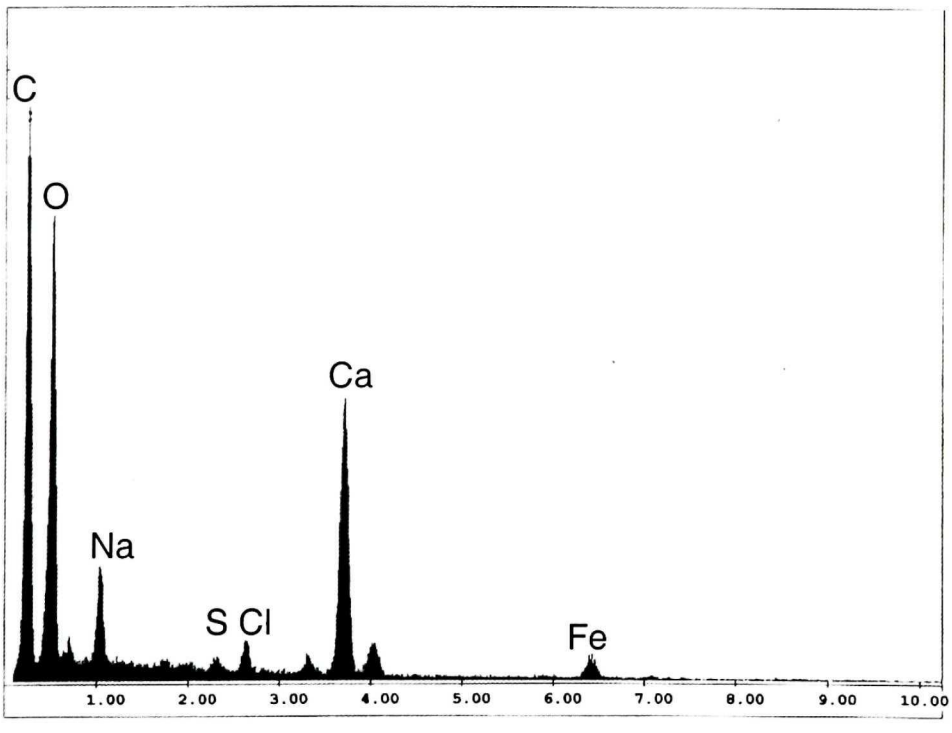

Figure 5.18 X-ray spectrum analysis of the spheroidal particle in Figure 5.14

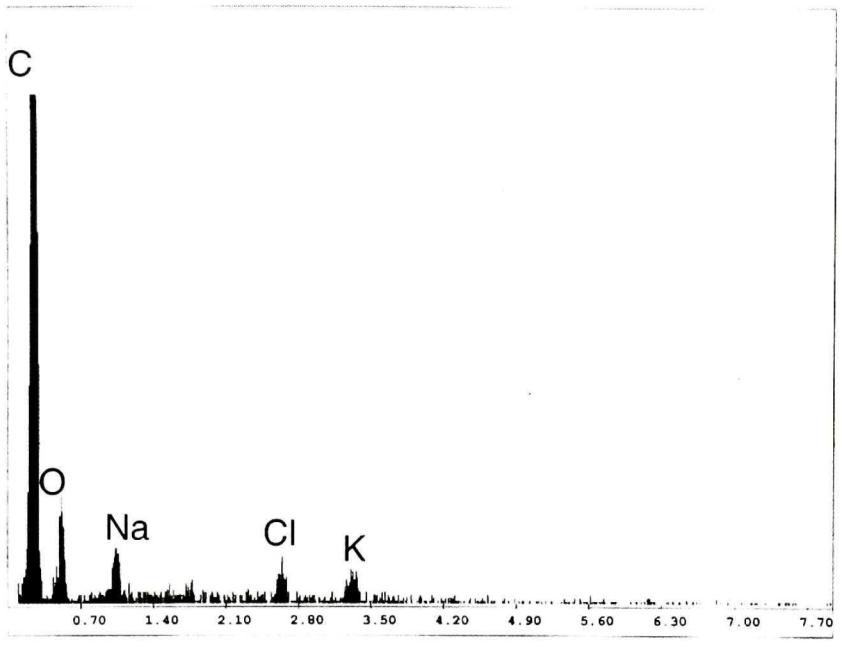

Figure 5.19 X-ray spectrum analysis of the particle in Figure 5.16

Figure 5.18 illustrates that the composition of the spheroidal particle presented in Figure 5.14 included C, O and Ca. Figure 5.19 is the X-ray spectrum of the particle in Figure 5.16, which is in a dimple on the fracture surface of an HT-I sample. The spectrum indicates that the particle is a carbide. The Na, Cl and K peaks are due to contamination of the fracture surface.

As discussed above, second phase particles lead to the initiation of fracture because of the stress concentrations caused by the differences in ductility between the particles and the matrix material. Particle B in Figure 5.15 is a carbide platelet that had been broken into pieces. A crack was initiated at one end and extended from it. Another example is shown in Figure 5.20. Two particles were located on the fracture surface of an HR sample. EDS analysis revealed that both particles are iron carbides, whilst the X-ray spectrum of the larger particle reveals the presence of a small S peak (Figure 5.21). A crack originated on the particles and then connected them up.

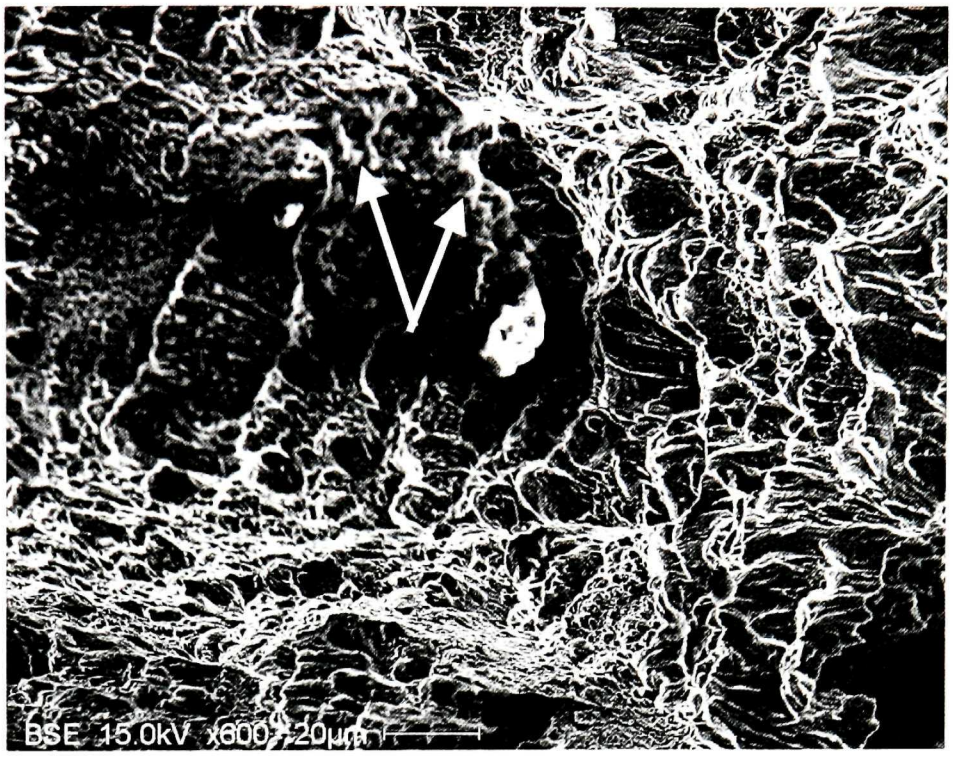

Figure 5.20 Carbide particles and a thin crack (arrowed) on the fracture surface of an HR sample, x600

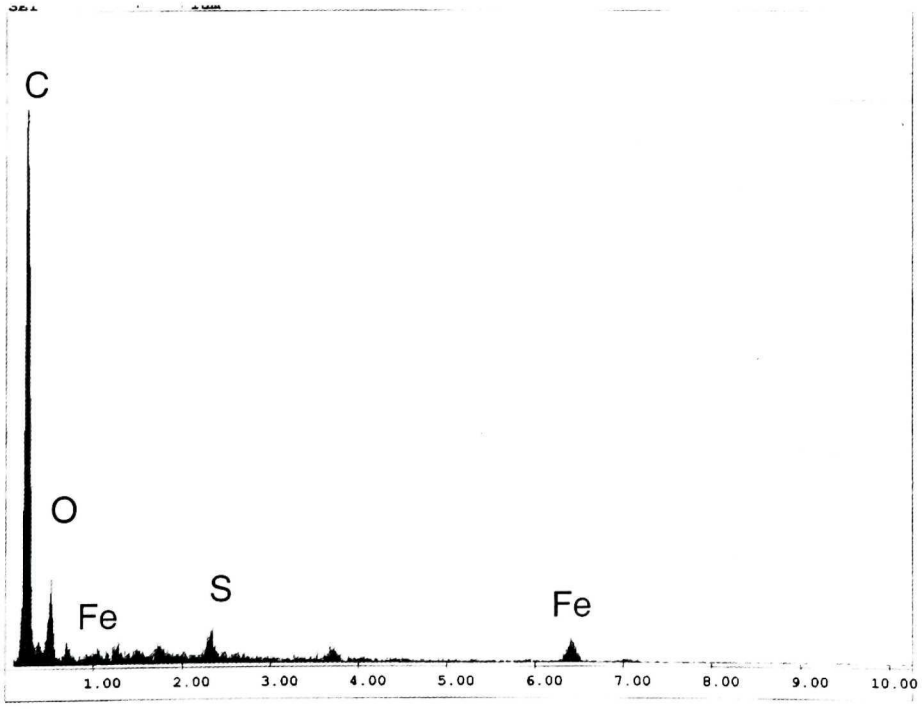

Figure 5.21 X-ray spectrum analysis of the large particle in Figure 5.20

Additional evidence was obtained from an HT sample. A small crack was present on the free surface of the sample at a magnification of x25 (Figure 5.22) and the crack was quite shallow. It is evident that the crack was initiated just below the surface. Under higher magnification, a particle was found on the crack and the fracture occurred at the interface between the particle and the matrix (Figure 5.23). EDS analysis indicated that this was a carbide. Thus a particle on or near the surface of a sample can act as a surface defect and then initiate a surface crack in this way.

A pearlite colony can also act as a stress concentration site and cause fracture during DWT. Figure 5.24 displays a pearlite colony on the fracture surface of an HR sample. The pearlite colony, located at the root of the fracture, was broken by the crack that penetrates through the colony.

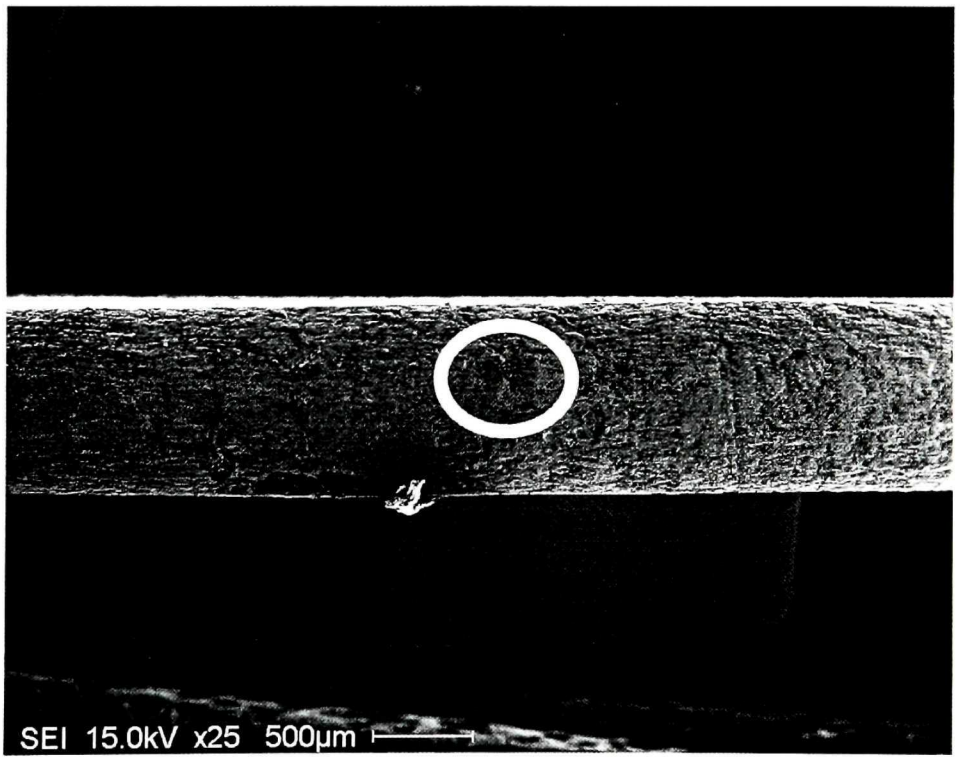

Figure 5.22 Small crack (circled) on an HT sample

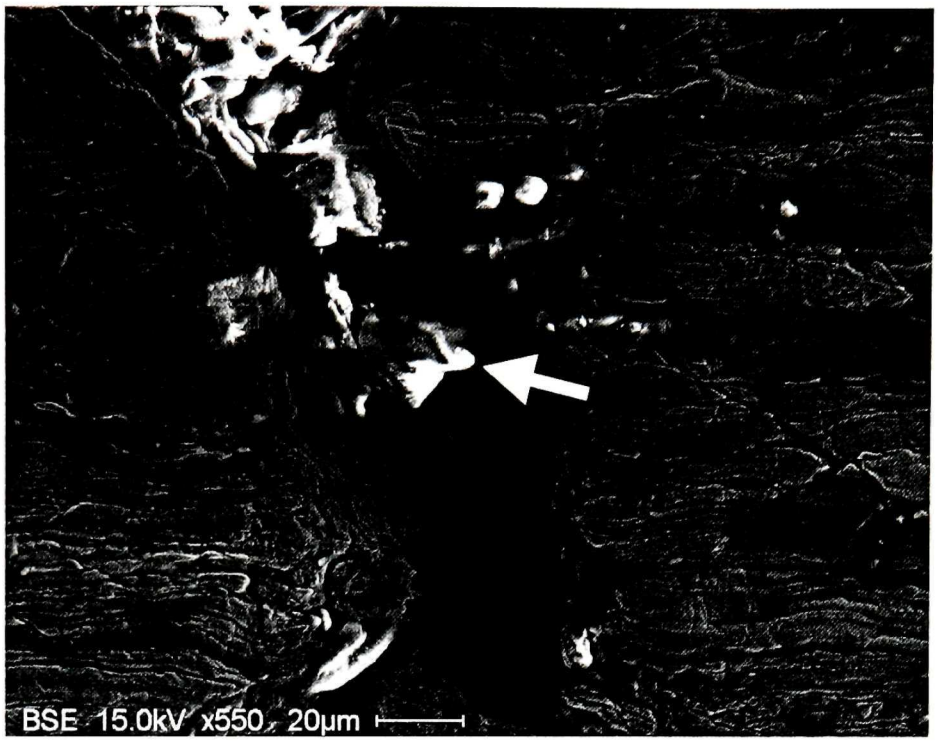

Figure 5.23 Higher magnification of the crack in Figure 5.22, carbide particle is arrowed, x550

Figure 5.24 Root area of the widely opened fracture in Figure 5.9, x300

During plastic deformation, voids nucleate at harder particles, then grow and coalesce during further flow of the matrix metal [Thomason, 1969; Narasimhan and Kamat, 1994]. The large particles fail by cracking while the smaller ones fail by interfacial decohesion [Van Stone et al., 1985]. That is why unbroken small particles were present at the fracture surface, while the pearlite colonies were cracked.

The growth and coalescence of voids depend on the flow instability of the matrix metal. During stable plastic flow, there is little potential for ductile fracture. Only when the tensile or shear instability condition of the matrix is reached does ductile fracture progress rapidly. The strain in the matrix from the moment of instability to fracture depends primarily on the proportion of second phase particles [Thomason, 1969]. The greater the second phase fraction, the lower the fracture strain. The HR microstructure had the highest proportion of the second phase; therefore it displayed the lowest fracture strains. By contrast, the HT-II material had the highest fracture strain and the lowest amount of second phase.

Although a few sulphide particles were found on some of the fracture surfaces, EDS analysis revealed that most of the second phase particles responsible for fracture in the DWT tests were carbides. In spheroidized microstructures, such as the HT-II and HT-III, the dimensions of the carbide particles were small as were their aspect ratios. This resulted in lower stress concentrations and higher ductility of the matrix. In relatively unspheroidized microstructures, such as those of the HR, HT and HT-IV samples, large amounts of the cementite were lamellar and of uneven dimensions. The platelet particles caused high stress concentrations during DWT; this resulted in early fracture. This is also the reason why microstructures containing spheroidal cementite possess better cold headability than those containing pearlite.

Chapter 6

Conclusions

1. The tests indicate that the drop weight test is able to differentiate between the cold headabilities of samples containing different microstructures. Therefore it is a valid method for assessing the suitability of materials for cold heading.

2. The cold headability of medium carbon steel is sensitive to the difference between the mechanical properties of the ferrite and the pearlite colonies. Therefore, it can be improved by reducing this disparity by means of heat treatment.

3. Cold headability is also sensitive to the inclusions and second phase particles contained in the microstructure. When such particles are present near the external surface of CHQ rod, they act as surface defects and lead to the nucleation of cracks.

4. The present results indicate that a totally spheroidized microstructure (the HT-II) has the best cold headability amongst the six tested microstructures.

References

Aihara, K. and Kanbara, S., 1990, "Influence of Prior Structure upon Spheroidization Rate and Cold Forge Ability of Annealed Wire", Sumitomo Search, No. 42. pp. 1-8.

Aihara, K., 1991, "A New Thermomechanical Processing for Spheroidizing Carbide Directly in a Rolling Line", 33rd Mechanical Working and Steel Processing Conference Proceedings, The Iron and Steel Society, Inc. (USA), pp. 285-290.

Baquet, I.G., Kaspar, R., Richter, J., Nussbaum, G. and Koethe, A., 1997, "Influence of Microalloying on the Mechanical Properties of Medium Carbon Forging Steels after Newly Designed Post Forging Treatment", Steel Research, No. 12, pp. 534-540.

Bickford, J. and Nassar, S., 1998, "Handbook of Bolts and Bolted Joints", M. Dekker, pp. 69-74.

Bruns, H. and Kaspar, R., 1997, "Pearlite Spheroidization by Thermomechanical Treatment of Directly Charged Thin Slabs", Steel Research, Vol. 68, No. 4, pp. 158-162.

Chattopadhyay, S. and Sellars, C.M., 1977, "Quantitative Measurements of Pearlite Spheroidization", Metallography, Vol. 10, No. 1, pp. 89-105.

Cockcroft, M.G. and Latham, D.J., 1968, "Ductility and Workability of Metal", Journal of the Institute of Metals, Vol. 96, pp. 33-39.

Cox, T.B. and Low, J.R. Jr, 1974, "Investigation of the Plastic Fracture of AISI 4340 and 18 Ni-200 Grade Maraging Steels", Metall. Trans., Vol. 5, pp. 1457-1470.

Das, T., Li, J.Y., Painter, M. and Summerville, E., 2002, "Evaluation of Two AISI 4037 Cold Heading Quality Steel Wires for Improved Tool Life and Product Quality", Journal of Materials Engineering and Performance (USA), Vol. 11, pp. 86-91.

El-Domiaty, A., 1999, "Cold Workability Limit for Carbon and Alloy Steels", Journal of Materials Engineering and Performance, Vol. 8, No. 2, pp. 171-183.

Fisher, J.R. and Gurland, J., 1981, "Void Nucleation in Spheroidized Carbon Steels", Metal Science, No. 5, pp. 185-192.

Floreen, S. and Hayden, H.W., 1970, "Some Observations of Void Growth During the Tensile Deformation of a High Strength Steel", SCR Met. Vol. 4, pp. 87-94.

Goods S.H. and Brown, L.M., 1979, "The Nucleation of Cavities by Plastic Deformation", Acta Metall. Vol. 27, No. 1, pp. 1–15.

Gurland, J., 1972, "Observation of the Fracture of Cementite Particles in a Spheroidized 1.05%C Steel Deformed at Room Temperature", Acta Metall., Vol. 20, pp. 735-741.

Gurland, J., 1988, "A Review of the Application of the Law of Mixtures to the Plastic Deformation of Two Phase Alloys", Israel Journal of Technology, Vol. 24, pp. 243-253.

Jenner, A. and Dodd, B., 1981, "Cold Upsetting and Free Surface Ductility", J. Mech. Work. Technol, Vol. 5, pp. 31-43.

Kohlmann, R., Kruse, M., Meyer, M. and Plociennik, U., 2000, "Optimization of Material Properties for Bars and Wire Rod", Metallurgical Plant and Technology Int., Vol. 23, No. 4, pp. 56-62.

Koyama, R., Higurashi, M., Fukusima, S. and Hagita, H., 1995, "Non-Heat-Treated Steel for Cold Forging Application", Recent Development of Rolling and Following Process Technology and/or Application of Steel Products, Penang, Malaysia, Session 10, pp. 4/1-4/15.

Kruse, M., Mauk, P.J. and Plociennik, U., 1996, "Temperature Control Conception for Thermomechanical Rolling in Bar and Wire Rod Mills-Plant Technology, Computer Simulation and Results", Metallurgical and Foundry Engineering, Vol.22, No. 3, pp. 183-198.

Kuhn, H.A., 1977, "Workability Testing and Analysis for Bulk Forming Process", Formability Topics - Metallic Materials, Toronto, Canada, American Society for Testing and Materials, pp. 206-219.

Lee, D.L., Lee, J.B., Kim, J.K. and Choi, J.H., 1992, "Steel Wire Rod for Cold Heading without Heat Treatment", SEAISI Quarterly (Malaysia), Oct., pp. 63-74.

Lee, P.W. and Kuhn, H.A., 1973, "Fracture in Cold Upset Forging - a Criterion and Model", Metallurgical Transactions Vol. 4, pp. 960-974.

Lehnert, W., 1995, "Production and Use of High Strength Cold Heading Steels", Wire (Germany) Vol. 45, No. 5, pp. 275-280.

Magnusen, P.E., Dubensky, E.M. and Koss, D.A., 1988, "The Effect of Void Arrays on Void Linking During Ductile Fracture", Acta Metall., Vol. 36, p.p. 1503-1509.

Maheshwari, M.D., Dutta, B. and Mukherjee, T., 1978, "Quality Requirement for Cold Heading Grades of Steel", Tool Alloy Steel, Vol. 12, p.p. 247-251.

Matsunaga, T. and Shiwaku, K., 1980, "Manufacturing of Cold Heading Quality Wire Rods and Wires", SEAISI, Quarterly, Vol. 9, No. 1, pp. 45-55.

Mazanec, K. and Mazancova, E., 1997, "Physical Metallurgy of Thermomechanical Treatment of Structural Steels", Cambridge International Science.

ASM Metals Handbook, 1992, "Interpretation of Scanning-Electron Microscope Fractographs", 8th ed., Vol. 9, pp. 64-78.

Muzak, N., Naidu, K. and Osborne, C., 1995, " New Methods for Assessing Cold Heading Quality", Wire Association International 65th Annual Convention, pp. 104-111.

Narasimhan, R. and Kamat, S.V., 1994, "A Numerical Investigation of Ductile Fracture Initiation in a High Strength Low Alloy Steel", Bulletin of Materials Science, Vol. 17, No. 3, pp. 259-282.

Nickoletopoulos, N., 2001, PhD Thesis, "Physical and Numerical Modeling of Steel Wire Rod Fracture During Upsetting for Cold Heading Operations", McGill University.

Nickoletopoulos, N., Hone, M., Wanjara, P., Verreman, Y., Nemes, J.A., Jonas J.J., and Yue, S., 2001, "Development of Fracture Criterion for Cold Heading", Wire Journal International, Vol. 34, No. 9, pp. 90-98.

O'Brien, J.M. and Hosford, W.F., 2000, "Spheroidizing of Medium Carbon Steels", Industrial Heating, Vol. 67, No. 9, pp. 79-82.

Ochi, T. and Koyasu, Y., 1992, "A Study of Spheroidizing Mechanism of Cementite in Annealing of Medium Carbon Steel", 33rd Mechanical Working and Steel Processing Conference Proceedings, The Iron and Steel Society, (USA), pp. 303-309.

Olsson, K., Karlsson, S. and Melander A., 1986, "The Influence of Notches, Testing, Geometry, Friction Conditions and Microstructure on the Cold Forge Ability of Low Carbon Steel", Scandinavian Journal of Metallurgy, Vol. 15, No. 5, pp. 235-256.

Peisker, D., Doktorowski, A., and Dittrich, D., 2001, "Contribution on the Influence of Transformation Structure Under Consideration of Austenite Deformation", Steel Research, Vol. 72, No. 3, pp. 111-114.

Pickering, F.B., 1980, "Some Aspects of the Relationships between the Mechanical Properties of Steels and Their Microstructure", TISCO, Vol. 27, pp.105-132.

Pittinato, G.F. (editor), 1975, "SEM/TEM Fractography Handbook", McDonnell Douglas Astronautics Company.

Poruks, P., Wilkinson, D.S. and Embury, J.D., 1998, "Role of Particle Distribution on Damage Leading to Ductile Fracture", ASM International, Analysis of In-Service Failures and Advances in Microstructural Characterization, Vol. 26 (USA), pp. 491-496,

Ray, A., Paul, S.K. and Jha, S., 1996, "Effect of Inclusions and Microstructural Characteristics on the Mechanical Properties and Fracture Behavior of a High-Strength Low-Alloy Steel", Journal of Materials Engineering and Performance (USA), Vol. 4, No. 6, pp. 679-688.

Ren, C. and Varo, R., 1999, "Controlled Cooling Process in the Tianjin High Speed Wire Rod Mill", Metallurgical Plant and Technology Int., Vol. 22, No. 4, pp. 88-93.

Sarruf Y., 2000, "Criteria and Tests for Cold Headability", Master's thesis, McGill University.

Sarruf, Y., Cao, B.H., Jonas, J.J. and Nickoletopoulos, N., 1998, "Criteria and Tests for Cold Headability", 68th Annual Convention of the Wire Association International, Wire Association International Inc., pp. 141-148.

Shah, J.J. and Kuhn, H.A., 1986, "An Empirical Formula for Workability Limits in Cold Upsetting and Bolt Heading", J. Appl. Metalwork., Vol. 4, No. 3, pp. 255-261.

Shockey, D.A., Curran, D.R. and Seamen, L., 1977, "Computer Modeling of Microscopic Failure Processes Under Dynamic Loads", Proc. Conf. of High Velocity Deformation of Solids, Tokyo, Japan, pp. 149-162.

Shore, S.M., Rixham, B. and Keyzer, PL., 1998, "Rod Mill Improvement for Increased Profitability", 40th Mechanical Working and Steel Processing Conference, Iron and Steel Society, Vol. 36, pp. 653-661.

Sun, Z.Q., Yang, W.Y., Hu, A.M., and Yang, P., 2001, "Deformation Enhanced Ferrite Transformation in Plain Carbon Steel", Acta Metall., Vol. 14, No. 2, pp. 115-121.

Thibau, R., Trudel, A., Baragar, D. and Hastings, P.R., 1999, "Development of a Test to Evaluate the Formability of CHQ Wire", Wire Association Int. 69th Annual Convention, Wire Association Int., pp. 232-241.

Thomason, P.F., 1968, "The Use of Pure Aluminium as an Analogue for History of Plastic Flow in Studies of Ductile Fracture Criteria in Steel Compression Specimens" , Int. J. Mech. Sci. 1968, Vol. 10, pp. 501-518.

Thomason, P.F., 1969, "Tensile Plastic Instability and Ductile Fracture Criteria in Uniaxial Compression Test", Int. J. Mech. Sci., Vol. 11, pp. 187-198.

Thomason, P.F., 1969/1970, "The Effect of Heat Treatment on the Ductility of Alloy Steel Wires in a Cold Heading Process", Proc. Inst. Mech. Engrs, Vol. 184, Pt. 1, No. 47, pp. 875-884.

Thomason, P.F., 1969B, "The Free Surface Ductility of Uniaxial Compression Specimens with Longitudinal Surface Defects", Int. J. Mech. Sci., Jan., pp. 65-73

Trufiakov, V.I., Kirjan, V.I. and Novikova, D.P., 1992, "Relationship between the Structure and Ductile Fracture Resistance of Ferritic-Pearlitic Structure Steel", Soviet Material Science, Vol. 28, No. 3, pp. 289-294.

Tsai, D.H., Jou, D.S., Hwang, I.S., Lin, H.R. and Guo, Y.T., 2000, "Development of Microalloyed Extra Low Carbon Steel Bars for Severe Cold Heading Quality", SEAISI Quarterly, Jul., pp. 19-34.

Van Stone, R.H., Cox, T.B., Low, J.R. and Psoda, J.A., 1985, "Microstructure Aspects of Fracture by Dimpled Rupture", Int. Met. Rev., vol. 30, No. 4, pp. 157-179.

Wanjara, P., Donaberger, R., Hone, M., Nemes, J.A., Nickoletopoulos, N, Tendler, A. and Yue, S., 1999, "Development of Application of Dual Phase Steels for Cold Heading High Strength Steel Fasteners", AIME 41st Mechanical Working and Steel Processing Conference, pp. 151-157.

Wick, C.H., 1960, "Chipless Machining", New York Industrial Press, pp. 34-71.

Wu, F., Liu, J., and Hu, J., 1999, "Rapid and Direct Spheroidization of Carbide in Hypoeutectoid Steels", Journal of National University of Defense Technology, Vol. 21, No. 6, pp. 27-31.

Yoo, S.J., Lee, D.L. and Chung, D.T, 1997, "Prediction of Cold Heading Quality with High Strain Rate Compression Test", Wire Journal Int., Vol. 30, No. 9, pp. 84-89.